AIAA SciTech Forum
4-8 January 2016, San Diego, California, USA
54th AIAA Aerospace Sciences Meeting

10.2514/6.2016-1029

Design Study for a Highly Fuel Efficient Regional Transport

Jeffrey Kirkman[1], Donald Wood[1], Tyler Knight[1], Michael Gurczak[1], Cameron Rothlisberger[1], Zhanxiao Pan[1]

and

Timothy T Takahashi[2]

Arizona State University, Tempe, AZ, 85281

This paper documents a study for a 70 seat regional transport jet aircraft that maximizes fuel efficiency. The aircraft must be significantly more economical than current market competitors, namely the Embraer E-170 and Bombardier CRJ-700. The design utilized the programs *ModelCenter* for trade studies and optimization, *EDET* for drag estimation, and *VORLAX* for stability and control. The final design, "*Aeris*", has a cruciform tail, low wing configuration, with four engines buried in the wing. This configuration has a cruise altitude of 50,000 ft at a Mach number of .83. The aircraft can complete a 1500 -nM with a 15,000-lbm payload in 3 hours 25 minutes while burning 5813-lbm of fuel. For a shorter 500 -nM mission with a 13,000-lbm payload, the aircraft completes the mission in 1 hour 33 minutes at a fuel burn of 2365-lbm.

[1] Undergraduate Student, Aerospace Engineering, School for Engineering of Matter, Transport and Energy, PO Box 8576016, Student Member AIAA.
[2] Professor of Practice, Aerospace Engineering. School for Engineering of Matter Transport and Energy, PO Box 8576106, Associate Fellow AIAA.

© 2016 – Kirkman, Wood, Knight, Gurczak, Rothlisberger, Pan and Takahashi

Copyright © 2016 by J.
J. Kirkman, D.L. Wood, T.H. Knight, M.Gurczak, C.Rothlisberger, Z.X.Pan and T.T.Takahashi. Published by the American Institute of Aeronautics and Astronautics, Inc., with permission.

Downloaded by Timothy Takahashi on May 11, 2023 | http://arc.aiaa.org | DOI: 10.2514/6.2016-1029

Nomenclature

AR	=	Aspect ratio
α	=	Angle of attack
b	=	Span
BEW	=	Basic empty weight
BPR	=	Bypass ratio
c	=	Chord
c_d	=	Coefficient of drag
c_{di}	=	Induced drag coefficient
c_l	=	Coefficient of lift
c_m	=	Coefficient of moment
$c_{m\alpha}$	=	Pitching moment stability derivative
$c_{n\beta}$	=	Yawing moment stability derivative
$c_{n\beta DYN}$	=	Dynamic directional stability derivative
c_p*	=	Critical Pressure Coefficient
c_{pmin}	=	Minimum Pressure Coefficient
CFL	=	Critical Field Length
d	=	Diameter
D	=	Drag
e	=	Oswald efficiency factor
Λ	=	Sweep angle
λ	=	Taper ratio
$KIAS$	=	Knots indicated air-speed
$KTAS$	=	Knots true air-speed
L	=	Lift
l	=	Length
lbf	=	Pound force
lbm	=	Pound mass
M	=	Mach number
M_{cr}	=	Critical Mach number
M_{div}	=	Drag Divergence Mach number
MLW	=	Maximum landing weight
$MTOW$	=	Maximum takeoff weight
$MZFW$	=	Maximum zero-fuel weight
OEW	=	Operational Empty Weight
ROC	=	Rate of climb
S_{ref}	=	Planform area
S_{wet}	=	Wetted area
t	=	Thickness
T	=	Thrust
v	=	Velocity
W	=	Weight

Downloaded by Timothy Takahashi on May 11, 2023 | http://arc.aiaa.org | DOI: 10.2514/6.2016-1029

Introduction

The fuel efficiency of commercial aircraft has improved over the years, but fuel cost is still by far the biggest expense for any airline. It is possible to offset these costs by filling more seats on each flight or by replacing older aircraft with newer, more fuel-efficient planes. Higher fuel efficiency results in lower costs of transport per person, allowing a larger profit margin for airlines, decreased ticket costs for passengers, or some happy median between the two.

Speed also plays an important role in air transport. Flight times are a major consideration for airlines due to the ability to complete more flights within an operational day. Additionally, shorter flights are more convenient for the passengers. A highly efficient aircraft is unlikely to be used if it flies too slowly resulting in longer mission times. A faster plane can complete more missions in a single day, meaning an airline can earn more ticket sales per day off of a single aircraft.

A regular topic of argument within the industry is weighing the merits of speed against efficiency. These design parameters do not necessarily need to be mutually exclusive. The ideal aircraft would incorporate both speed and efficiency in its design and operation.

One specific market in the air travel industry that could greatly benefit from more efficient aircraft is that of the regional jet. Regional transports are used for short to medium range missions and typically carry 60-90 passengers. With less room than larger, long-haul aircraft to fit passengers, fuel efficiency is key to lowering the fuel cost per passenger. This market has several current offerings, but there is plenty of room for future competitors. Any new design would need to be competitive in terms of flight speed, cabin comfort, and field performance, while improving fuel economy. This was the task undertaken in designing the *Aeris.*

I. Design Process, Goals and Requirements

Before the design process began, several constraints were put in place so that the final product would be a viable alternative to the current competitors. In order to be comparable in terms of basic room and comfort the aircraft had to carry 2 pilots, 2 cabin attendants, and 68 to 70 passengers in a typical 2-class interior. To have competitive flight times the plane was to be designed to cruise at a Mach number of at least 0.70. For airport use, the aircraft had to be able to take off in less than 5000-ft and land in less than 4000 ft. The aircraft was to be sized for a 1500-nM mission

with a 45 minute hold while carrying 15,000-lbm payload. In addition, the design had to achieve maximum economy while flying a shorter range mission of 500-nM.

Various software tools were built and verified in order to complete the project within the time allotted. Although the methods used were first order tools, they were verified using manufacturer's data [1][2][3][4][5][6] of existing planes in order to prove that the outputs were consistent with the results of flight test data. This verified that the tools were sufficient for the design process. After the various tools were built and tested, they were used together in conjunction to take statistical samplings and find a design that complied with the constraints. We verified our final design against these performance, fuel burn, sizing, stability, and certification metrics.

The overall goal of the project was to design a regional transport jet that is more efficient than the current market competitors. In addition to this broad stroked requirement, there were specific target goals for the aircraft. The goals were as follows:

- Carry 2 pilots, 2 cabin attendants, and 68 to 70 passengers in a typical 2-class interior
- Cruise at Mach 0.70 or higher
- Complete the following "longer-range" mission
    - 1500-nM climb/cruise/descent plus 45 minute hold at 5,000-ft with a 15,000-lbm payload
    - Takeoff CFL less than 5,000-ft at MTOW
    - Landing Distance less than 4,000-ft at typical landing weight
- Complete the following "shorter-range" mission (with take-off at less than MTOW)
    - 500-nM climb/cruise/descent plus 45 minute hold at 5,000-ft with a 13,000-lbm payload
    - Landing Distance less than 4,000-ft at typical landing weight
- Meet 35-lbm fuel consumed per seat on the 500-nM trip with 13,000-lbm payload

The top level design process for the project is shown in Figure 1. More detailed flowcharts for each component will be provided in the later design sections. The fuselage was the initial starting point, since the crew and passenger accommodations are key sizing factors. The team then designed the wing according to this proposed fuselage, which fed into determining the weight of the craft. The engine size and tail volumes were simultaneously determined based on the weight estimation tool output. With these values found, members tested the aircraft's stability and then proceeded to see if it completed the necessary missions within the constraints. The process was very circular, with most aspects influencing the others. It was because of this that many times this process was treated more as a guideline and not a strict procedure to be followed exactly.

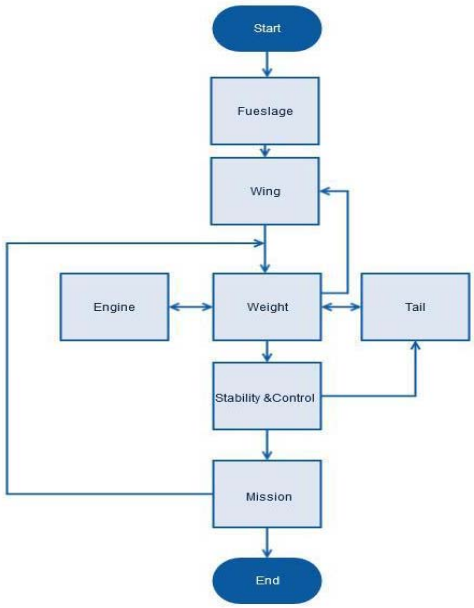

Figure 1. Design Process.

Downloaded by Timothy Takahashi on May 11, 2023 | http://arc.aiaa.org | DOI: 10.2514/6.2016-1029

As a form of commercial transport, the aircraft is also bound to the Code of Federal Regulations for certified flight operations within the United States [7]. The corresponding federal aircraft regulations are found in Title 14: Aeronautics and Space, with the majority of the regulations necessary for this aircraft are located in 14 CFR Part 25: Transport Category Airplanes. All design requirements and federal regulations were organized into a Requirements Traceability Matrix (Figure 2). This broke down the requirements for the various components of the aircraft and mission. This matrix allowed for quick verification of compliance.

REQUIREMENTS TRACEABILITY MATRIX

Project Name:	Aeris
Class:	AEE 468
Project Manager Name:	Team 1
Project Description:	Regional Jet

ID	Assoc ID	Technical Assumption(s) and/or Customer Need(s)
		MISSION
001	Long Rang Mission	1500-nm climb/cruise/descent + 45 min hold at 5,000-ft w/ 15,000-lbm payload
002	Long Rang Mission	Takeoff CFL < 5,000-ft @ MTOW
003	Long Rang Mission	Landing Distance < 4,000-ft @ typical landing weight
004	Short Range Mission	500-nm climb/cruise/descent + 45 min hold at 5,000-ft w/ 13,000-lbm payload
005	Short Range Mission	Landing Distance < 4,000-ft @ typical landing weight
006	Short Range Mission	35-lbm fuel consumed per seat on 500-nM trip w/ 13,000-lb payload
007	Cruise	Cruise at M = 0.7 or faster
14 CFR §25.103	Stall Speed	Vsr >= Vcl_max/sqrt(n_zw)
14 CFR §25.107	Takeoff speeds	Speeds required for takeoff
14 CFR §25.109	Accelerate-stop distance	Must be able to brake in time on a rejected takeoff
14 CFR §25.121	Climb: 1 engine Inoperative	Must be able to complete climb with an engine out and beyond the rejected takeoff zone
		ENGINE
14 CFR §25.367	1 Engine Inoperative	Designed to handle unsymmetrical loading if 1 engine fails
14 CFR §25.903	Engine Isolation	Engine failure cannot prevent the safe operation of the other engines
		STRUCTURE
14 CFR §25.305	Factor of Safety	Unless otherwise specified, use a factor of 1.5
15 CFR §25.333	Strength and Deformation	Structure must be able to support limit loads without detrimental, permanent deformation and deformation up to limit must be safely operable
16 CFR §25.303	Flight Manuevering Envelope	See diagram
		WINGS AND EMPENNAGE
14 CFR §25.143	Controllability & Maneuverability	Must be safely controllable and maneuverable through takeoff,climb, level, descent, & landing (see chart for exact settings)
14 CFR §25.147	Directional & Lateral Control	Must be able to yaw into inoperative engine with wings level and in full landing configuration
14 CFR §25.149	Minimum control speed	Minimum control speed cannot exceed 1.13 stall speed
14 CFR §25.181	Stability	Must be longitudinally, directionally, and laterally stable during all sections of flight
14 CFR §25.171	Dynamic Stability	Short period oscillations must be heavily damped with free & fixed controls
14 CFR §25.203	Stall Characteristics	Must produce/correct roll and yaw by unreversed aileron & rudder controls
14 CFR §25.337	Limit Manuever Load Factor	Positive limit maneuvering load n factor may not be... Less than 3.8
		FUSELAGE
008	Payload	Carry 2 Pilots, 2 cabin attendants, and 68-70 passengers
009	Payload	2 Class Interior

Figure 2. Requirements Traceability Matrix.

With the requirements organized, the team determined how the aircraft's flight characteristics would correspond to these needs. The team developed a House of Quality (Figure 3) to graph the relationships between these aspects. On the right side of this document, are the competitor's values, many of which were estimated. The main purpose of this document was to be able to link the requirements to their functional counterparts, and to track these characteristics against our competitors.

Downloaded by Timothy Takahashi on May 11, 2023 | http://arc.aiaa.org | DOI: 10.2514/6.2016-1029

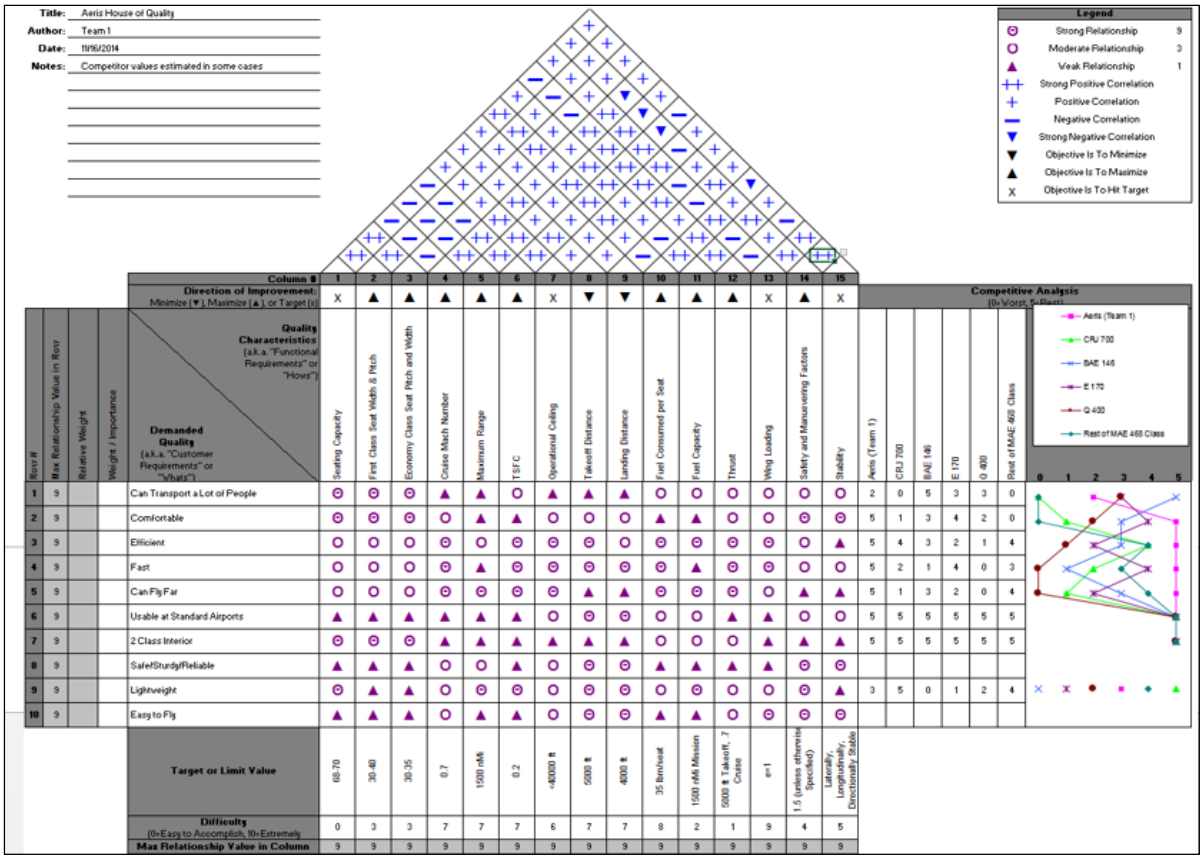

Figure 3. House of Quality.

II. Design Tools and Verification

Various software tools were built and verified in order to complete the project within the time allotted. The key tools used in the design of the aircraft are described below.

A. Torenbeek Weights Spreadsheet

The team utilized Professor Torenbeek's empirical weight estimation equations from his book *Synthesis of Subsonic Airplane Design* [8] as coded into spreadsheet form. From a collection of basic factors, dimensions and other geometry descriptors of an aircraft, these equations can compute an estimate of weights (BEW, OEW, MZFW, etc.). For verification of the spreadsheet, the team tested the geometry of the Boeing 737-300 and 747-100. The results from the spreadsheet maintained percent errors of less than 1% compared to the weights published by Boeing in their "Airplane Characteristics for Airport Planning" for the 737[4] and 747[5].

B. *EDET* (Empirical Drag Estimation Technique)

To determine the drag for the aircraft design, the team used *EDET,* an acronym for empirical drag estimation technique. *EDET* is a FORTRAN code that was developed in the 1970s by Lockheed for NASA. The user inputs the aircraft geometry as well as flight altitude and Mach number, with outputs returning, skin friction and profile drag of the various components along with lift induced drag. Verification was once again run using the geometries of the Boeing 737-300[4] and 747-100[5]. This verification allowed the team to select the optimal "crud factor" to account for any additional excrescences. The factor that best correlated theoretical and actual flight values was 25%. This was the "crud factor" that was incorporated into the project design.

Downloaded by Timothy Takahashi on May 11, 2023 | http://arc.aiaa.org | DOI: 10.2514/6.2016-1029

C. *VORLAX*

The code used to determine the stability and control of the aircraft was *VORLAX*. It is a vortex lattice method used to solve for forces generated on an airframe in flight. Developed by Lockheed under contract for NASA, *VORLAX* has been available for use since the 1970s [9]. Users input the geometry of the aircraft as a series of flat plate panels, cambered panels, or sandwiched panels. The code computes total airframe forces and moments including stability derivatives, as well as detailed wing pressure and normal force distributions. While *VORLAX* was vital to the design of *Aeris*, care had to be taken during the design process as the software only models attached flow. Therefore, stall or regions of unattached flow are not modeled. The team verified this tool by testing the geometry of the Boeing 737-300 at various Mach numbers and angles of attack, and obtained values very similar to those publish from flight test data. Flight stability and field performance was evaluated with 2D cambered wing panels, as this simpler model was less time consuming for the computer to compile. For flight conditions around cruise and higher subsonic Mach numbers, a more complex sandwich panel was used for evaluation. The sandwich panel model simulated the wing geometry with a cambered upper and lower surface. This allowed for aerodynamic analysis of the wing based on camber and thickness parameters which have large effects on the critical pressures and triggering of drag divergence.

D. Engine Data

We used NASA's Numerical Propulsion System Simulation (*NPSS*) to generate propulsion data for use in all aircraft performance calculations. *NPSS* simulates a two-shaft turbofan engine. For each engine (defined by turbine inlet temperature, operating pressure ratio, fan pressure ratio, reference bypass ratio), *NPSS* was run successively over a range of flight speeds, altitudes, and power settings. This process builds a series of databases of "five column performance data"

Many models were available to the design team. They represented different types of high bypass ratio turbofan engines from *BPR* = 4.7 through *BPR*= 12. The *BPR* 4.7 engine is roughly equivalent in technology to the CFM 56 engine featured on the B737; *OPR* = 33:1; *T4max* = 2300°F, *FPR*=1.6. The *BPR* 12 engine is roughly equivalent in technology to the Rolls Royce Trent XWB engine featured on the A350XWB; *OPR*=50:1; *T4max* = 2900°F, *FPR*=1.6.

"Five column performance data" comprises tables of net thrust (*Fn*) and thrust-specific-fuel-consumption (*TSFC*) as functions of altitude, Mach, and Power Setting. The altitude varied from sea level to 55,000 feet, a Mach of 0 to 1.0, and power level settings of 85% to 100% of *N1max* (10,000 rpm). *NPSS* produced normalized thrust data for an engine with 10,000-lbf sea-level standard day static thrust. For design purposes, this engine was "rubberized" using a scale factor to provide an adjustable thrust output for the aircraft design.

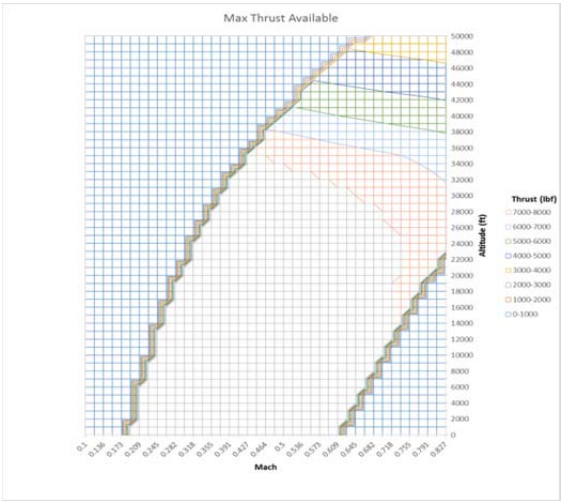

Figure 4. Thrust lapse with speed and altitude – BPR 12.0 turbofan

Downloaded by Timothy Takahashi on May 11, 2023 | http://arc.aiaa.org | DOI: 10.2514/6.2016-1029

E. SkyMaps

The *SkyMaps* tool utilized *NPSS* five-column engine data, and *EDET* output data to calculate performance parameters such as c_l, c_d, L/D, drag, M(L/D), fuel flow, specific range, and ROC. Each of these were calculated for a range of altitudes and Mach numbers and then displayed as a contour plot. These plots made it possible to determine the best performance points that would be incorporated into the mission profile. For example, the best cruise altitude and Mach number for optimizing specific range could be determined.

F. ModelCenter

ModelCenter is an essential tool to enable optimization and trade studies. This software was developed by Phoenix Integration. This software is able to integrate and interface with other programs, such as MATLAB or Microsoft Excel. Data from different components can be integrated into a single system model. It allows inputs and outputs to be specified and connected together, so, for instance, the outputs of one Excel file can be linked into the inputs of another. *ModelCenter* allows the users to vary the values of any of these inputs/outputs, and through this it allows the running of parametric studies, carpet plots, probabilistic analysis, etc. The team's primary use of *ModelCenter* was for linking all the tools (*EDET, VORLAX, SkyMaps*, etc.) and running trades that contained copious amounts of data points.

G. Mission Code

The mission code utilizes a VBA script that ran behind Excel to fly a chosen aircraft configuration through a specified mission profile. For its inputs, it used *EDET* output data, NPSS 5-column engine data, and a mission profile script. It calculated the fuel burned, time flown, distance flown, airspeed, Mach, ROC, and other performance parameters throughout the flight of the mission. This code made it possible to tweak the mission parameters and find the best altitudes and speeds at which to fly in order to minimize fuel consumption and verify that the given aircraft configuration can meet the mission requirements. The team verified this tool by creating a payload range curve for the Boeing 737-300, which was comparable to the one presented by the manufacturer.

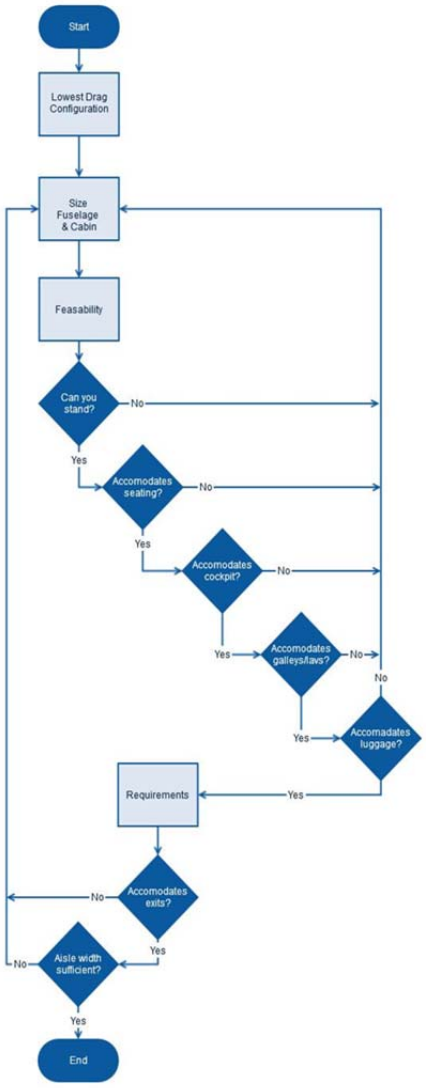

Figure 5. Fuselage Design Flowchart

III. Design

A. Fuselage

The design of the aircraft began with the sizing of the fuselage since this component allowed the aircraft to carry the required passenger compliment and required payload, and this portion of the design was least likely to be affected by the other design decisions. Fuselage design began with drag minimization, and is subsequently followed by testing of the feasibility and ability to meet CFR requirements. This process is demonstrated in Figure 5.

In sizing the fuselage, we observed the major design driver was the seating layout within the cabin. Varying the seats per row, seat width, and seat pitch were therefore, major fuselage dimensional drivers. The process began with sizing the fuselage and evaluating the drag using *EDET*, then checking for feasibility, such as appropriate cabin height, luggage space, minimum aisle widths, etc. These parameters were varied and analyzed using *ModelCenter*, and the lowest drag configuration was evaluated as the starting point for the design process. This initial design space consisted of over 30,000 combinations between seats per row, seat width, and seat pitch between first class and coach compartments (Figure 6).

Downloaded by Timothy Takahashi on May 11, 2023 | http://arc.aiaa.org | DOI: 10.2514/6.2016-1029

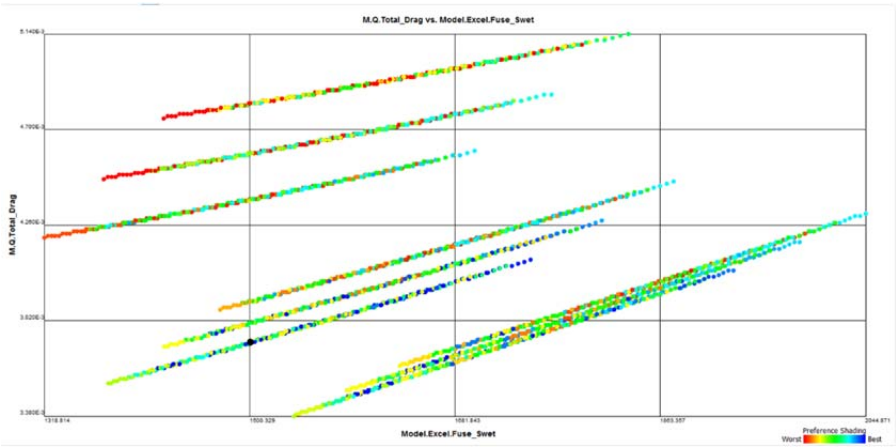

Figure 6. Initial Fuselage Study.

While this was a thorough evaluation of possible configurations, we discovered that the lowest drag configuration was a very impractical seating layout. In fact, many of the returned cabin configurations were very nonsensical, such as more seats per row in first class than coach. Upon further analysis, it was noted that the coach cabin width, in a common sense layout, was always larger than the first class cabin width, and therefore the primary driver in the fuselage width sizing. The fuselage trade study was then reevaluated and constrained to let the coach seating layout be the major dimensional driver for the cabin width while the seating pitch between first class and coach drove the length of the cabin.

Once the revised trade study (Figure 7) had been run, the practicality of the resultant configurations were evaluated beginning with the lowest drag configuration. The lowest drag configuration offered very low drag values which limited the seats per row at two across. However, the fuselage dimensionally was very impractical in that an average person would not be able to stand within the prescribed cabin height. Therefore, all of the two seats per row configurations were discarded. It was then found that the three seats per row in coach and two seats per row in coach was the lowest practical drag configuration.

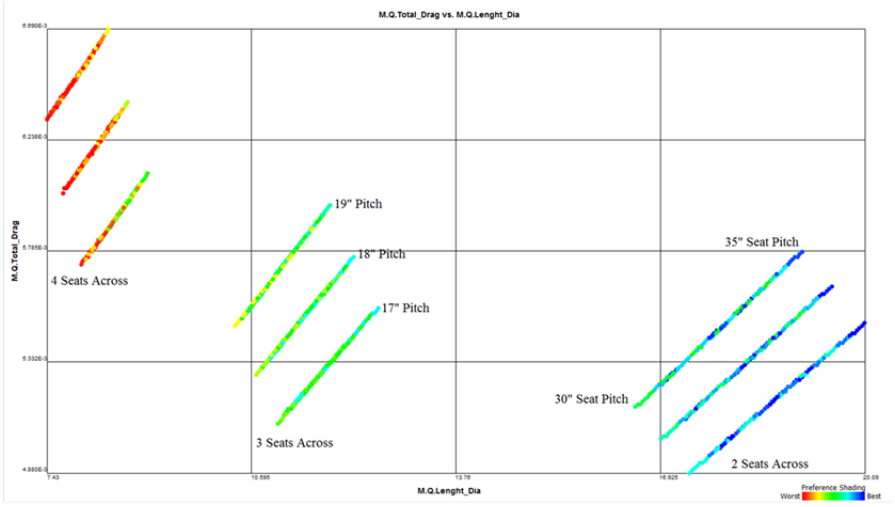

Figure 7. Revised Fuselage Trade Study.

In these fuselage trade studies, we simplified the fuselage as a cylindrical tube. However, as the initial sketches of the fuselage cross-section were being made it became clear there would be insufficient space for storing cargo (e.g. checked baggage). The decision had to be made of where to store the cargo within the fuselage. Possible configurations included, extending the fuselage in order to add a baggage compartment behind the main cabin (e.g. CRJ-700), or adding extra cross sectional area under the cabin floor to in order have a belly compartment for baggage (e.g. E-170). The possible configurations were evaluated for drag characteristics and the larger cross-sectional area,

Downloaded by Timothy Takahashi on May 11, 2023 | http://arc.aiaa.org | DOI: 10.2514/6.2016-1029

with a belly compartment, was found to be the lower drag configuration. After the extra cross-sectional area was added and the fuselage dimensions were adjusted it was discovered the cabin had gained enough width to accommodate four coach seats per row and three per row in first class. This had the effect of removing extra rows from the cabin layout which freed up room for galley/lavatory integration. After all of these iterations, the resultant fuselage was designed with the lowest possible drag configuration while still maintaining adequate cabin dimensions for passenger comfort and CFR requirements. The cabin orientation can be seen in Figure 8.

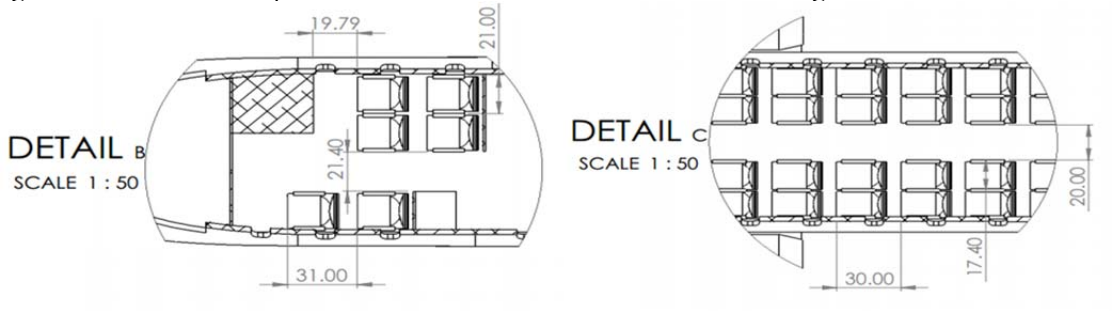

Figure 8. First Class & Economy Seating.

Type A emergency exits were fitted to each side of the fuselage in accordance to 14 CFR 25.807[10]. In order to conform to the 60-ft requirement (see Figure 9), the team decided to place the forward exit door mid cabin and the aft exit doors behind the final seat row. This creates an intimate first class compartment ahead of the boarding doors; while saving the weight and complexity of over-wing exits.

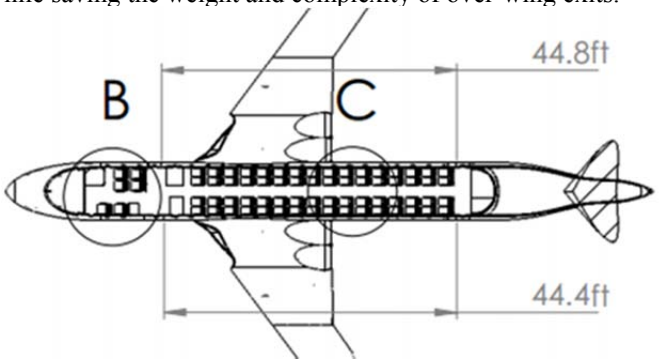

Figure 9. Emergency Exits.

B. Wing

The initial geometry of the wing was determined based upon trades run through *ModelCenter* in order to determine the effects on total aircraft performance. The initial wing design process is shown in Figure 10. These trades were run by varying the reference area, taper ratio, and sweep angle in order to understand their effects on the specific range, takeoff and landing performance, as well as cruise altitude and Mach number. In the initial trades there were 800 to 1000 combinations of these variables which gave some interesting results. The wing area mainly affected the takeoff and landing performance, however, it did have effects on the cruise point as well. The main effect on the specific range was determined to be from the Aspect Ratio, more specifically the observation that specific range increased with increased Aspect Ratio, resulting in increased span. Figures 11 and 12 show the results of the initial trades and the relationship between the various parameters and the specific range.

The first trades gave a rough overview of the planform, but this had to be refined as the aircraft weight and cruise points changed due to variations in other aircraft parameters. The results of the initial trades were used in order to resize the wing as these parameters changed. The team used this to decide upon the Aspect Ratio of the wing as well as the wing area for takeoff and landing field performance.

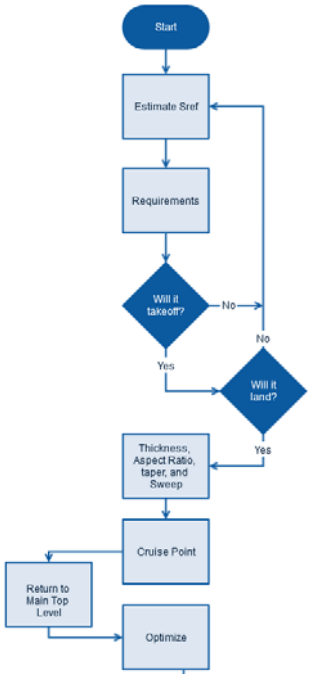

Figure 10. Initial Wing design Flowchart.

Downloaded by Timothy Takahashi on May 11, 2023 | http://arc.aiaa.org | DOI: 10.2514/6.2016-1029

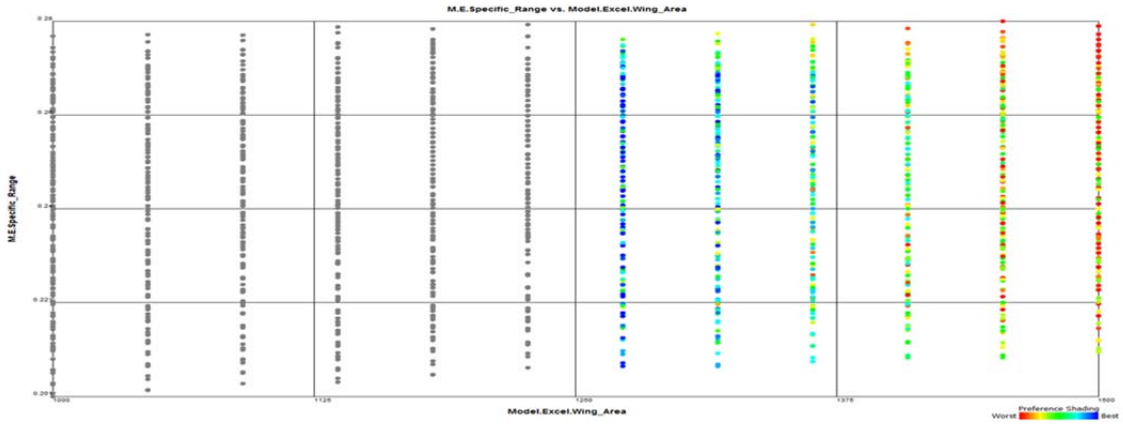

Figure 11. Specific Range vs Wing Area.

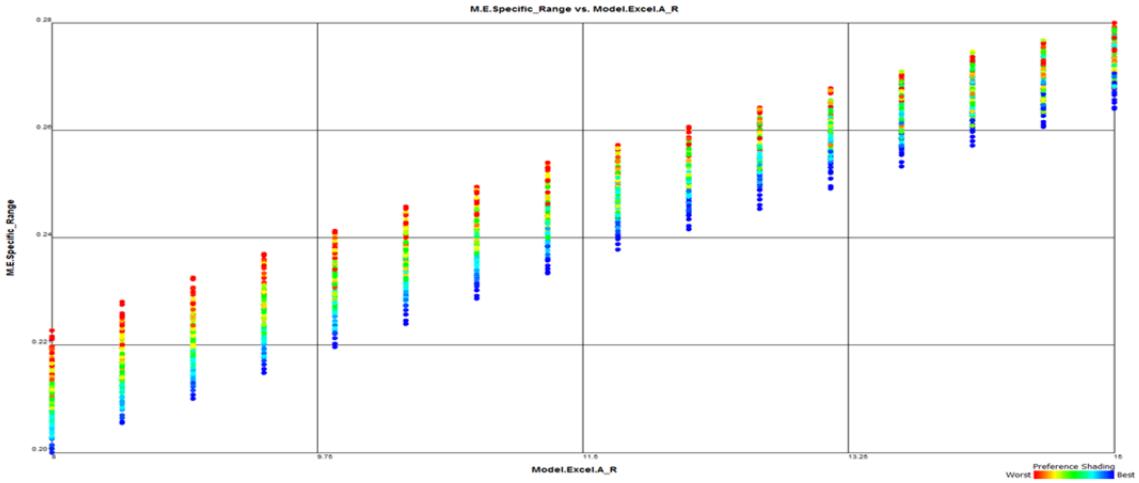

Figure 12. Specific Range vs Aspect Ratio.

Once the team decided that the top level geometry was reasonable and had converged with the rest of the design, the detailed wing design (Figure 13) began.

The detailed wing design includes the camber, twist, and thickness distribution of the wing in order to meet the design criteria set by the design team. The goals set for the wing were to:

- Meet the design lift coefficient
- Meet the desired cruise condition
- Achieve an elliptical lift distribution for low induced drag
- Achieve a favorable pressure distribution to maximize leading-edge suction

The detailed wing design process followed the one suggested by Takahashi & Donovan [11]. It began by determining the pressure coefficient relative to freestream that indicated sonic flow had been reached on the wing. This point correlates to what is commonly referred to as the critical pressure coefficient (c_p*). The team used the method set forth by Takahashi, Dulin, & Kady [12] to determine the critical pressure coefficient to be -0.45, therefore the peak underpressure on the wing was set to be -0.45 in order to achieve the critical Mach number at the designed cruise speed.

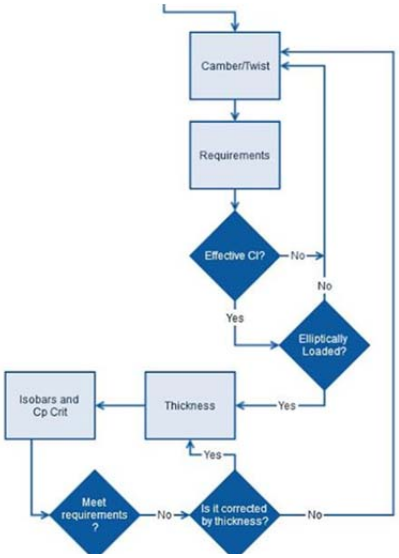

Figure 13. Detailed Wing Design Flowchart.

Downloaded by Timothy Takahashi on May 11, 2023 | http://arc.aiaa.org | DOI: 10.2514/6.2016-1029

The design team first attempted a wing design using a Whitcomb-style aft cambered section. During this initial design process, it became clear that the wing would have to be designed to cruise with the wing operating with significant supercritical flow; the design peak underpressure on the wing correlated to a local flow speed of Mach 1.2. While this might work, the team did not care for the strong nose-down pitching moment of the aft cambered airfoil which would result in significant trim drag. This lead the team to design the wing with a Pearcey peaky leading edge style camber line and a greatly reduced nose-down pitching moment.

The Pearcey peaky leading edge airfoil has some unique advantages over the Whitcomb aft-cambered airfoil. Primarily, the airfoil produces less pitching moments due to the center of pressure being located much closer to the airfoil pitching axis when compared to an aft cambered airfoil. Also, the airfoil has a decrease in drag at the critical Mach number because it is able to utilize the sonic flow to help improve leading edge suction [13]. Due to this the design changed from aft camber, to a *NACA a=0* camber line, which moved the maximum camber location toward the front section of the airfoil.

Once the team decided upon the camber line, the wing was segmented into five panels with six control points. The camber line was scaled at each control point and used in conjunction with the incidence (wing twist) to achieve an elliptical lift distribution across the wing. This process was done iteratively in order to obtain the desired lift coefficient while maintaining elliptical loading across the wing. Figure 14 shows the spanwise loading of the wing as well as the spanwise loading of the wing plotted against theoretical elliptical loading.

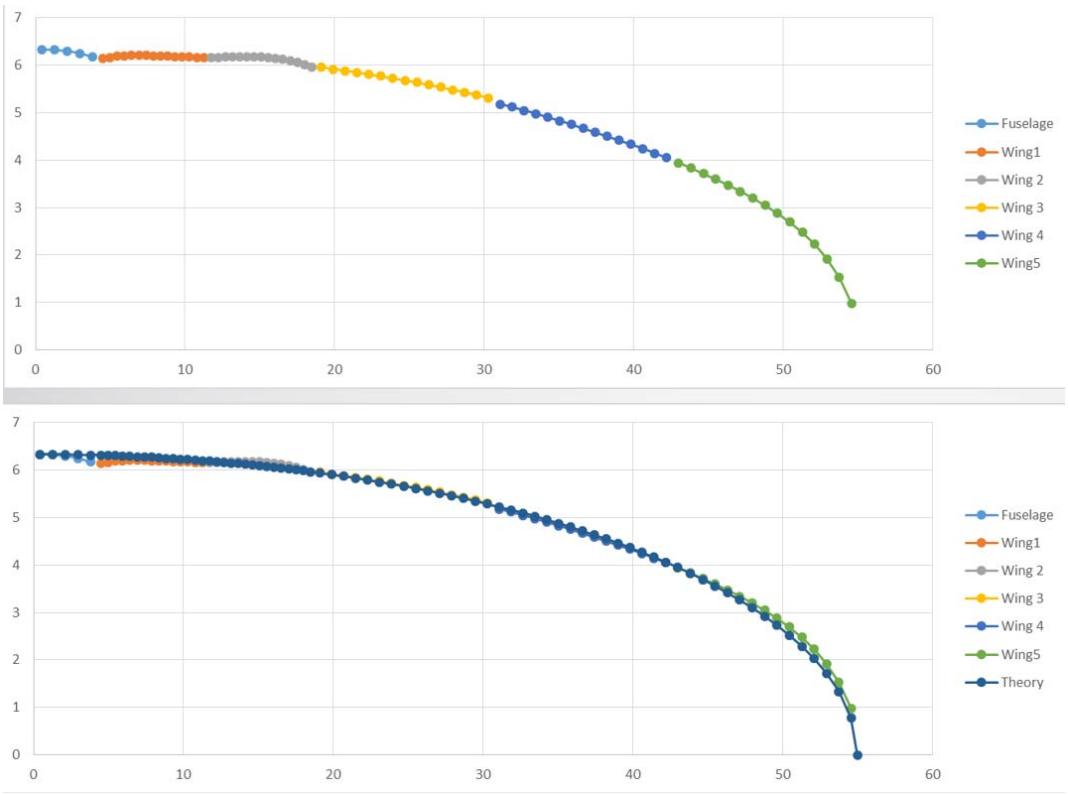

Figure 14. Spanwise Wing Lift Distribution.

The next step was to determine the thickness of the airfoil in order to achieve the favorable pressure distribution across the upper surface. The team decided on the NACA 66 thickness form due to the max thickness, hence the peak underpressure, occurs at the 60% chord. The synergism between camber and thickness form allows for the thickest possible wing while maintaining the desired upper surface pressure distribution. This strategy was utilized in order to reduce structural weight as much as possible.

Downloaded by Timothy Takahashi on May 11, 2023 | http://arc.aiaa.org | DOI: 10.2514/6.2016-1029

In order to determine the thickness distribution across the span, the Korn equation was used. This gave a starting point in order to determine the pressure distribution, however it became evident early on that the wing could be aerodynamically thicker than the results from the Korn equation.

The final step was to check the pressure distribution to ensure that the peak underpressure on the wing was met, and that the distribution of the pressures followed the leading edge sweep angle. This step was more of a checkpoint for the design, and if the standards set were not met then the process had to be repeated in order to adjust the wing. The wing was only considered finished once a favorable pressure distribution, shown in Figure 15, was achieved.

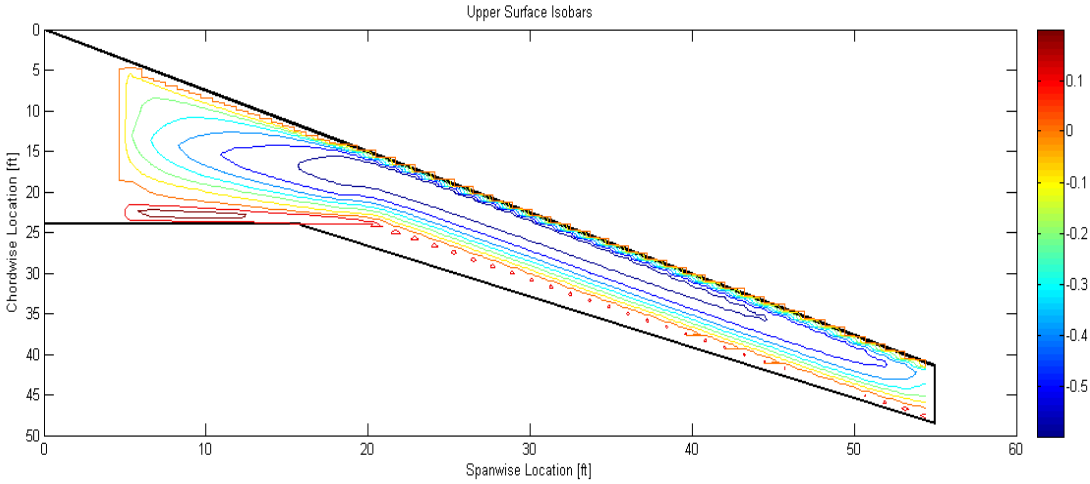

Figure 15. Upper Wing Surface Isobar

The final wing camber, twist and aerodynamic thickness are shown in Table 1. One of the notable aspects of the design is the root is a reflex cambered section (reminiscent of Boeing 707, 727 and Lockheed L-1011). This was essential to providing the favorable pressure distribution, because of the effect of having extra chord length in the wing's Yehudi area. In this portion of the wing the pressures tended to unsweep which was not desired. The other notable aspect of this design is the aerodynamic thickness of the wing. Since the wing has a buried engine design, this thickness does not include the engines, since the streamtubes are removed from the ensemble [14].

Table 1. Wing Twist, Camber, and Thickness.

Control Point	Twist	Camber	Thickness
Wing-Fuse Junction	3.35°	-30%	18%
1	1.5°	10%	15%
2	1.3°	67%	8%
3	0.2°	67%	8%
4	-1.6°	74%	8%
Wingtip	-4.2°	75%	8%

Due to the high thrust loading of the engines, and the large planform area, the aircraft does not need a complicated flap system to satisfy the filed performance requirements. It was determined that an increase of 0.8 in the coefficient of lift was necessary to meet the landing requirement. In the interest of simplicity of design, the team decided to explore the option of split flaps on the wing. Wenzinger's research [15] on split flap versus ordinary flap showed that it is possible to achieve an increase in lift coefficient of 1.1. In a split flap design there are no flap tracks, no large fairings, and the actuators are more simplistic. For these reasons the team decided that the split flap option would be much more practical than a complicated flap system.

The wing structure itself is designed classically, with main spar box ribs and stiffeners. The structure was built up in *Excel* as a finite element model that calculates the forces across the span. Some of the results from this spreadsheet are shown below in Figure 16.

Downloaded by Timothy Takahashi on May 11, 2023 | http://arc.aiaa.org | DOI: 10.2514/6.2016-1029

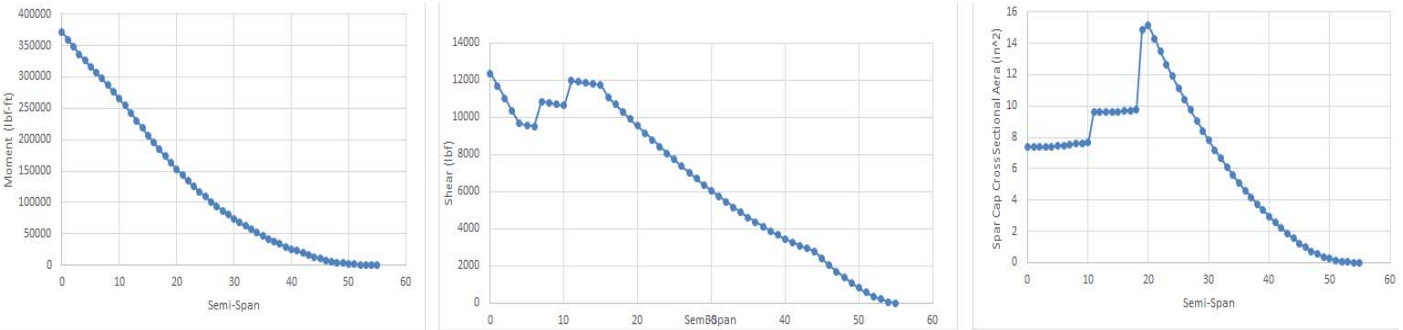

Figure 16. Moment, Shear, and Cross Sectional Area vs Span

There are two spars in the wing, one following the leading edge and the second along the trailing edge. These spars are sized to carry most of the load across the wing with ribs and stiffeners placed along the wing to help prevent buckling of the structure. The proposed fuel tanks sit on the outboard sections of the wing and underneath the engines. The fuel tanks sit within the spar box upper and lower surfaces, and are sized in the area between the spars (Figure 17).

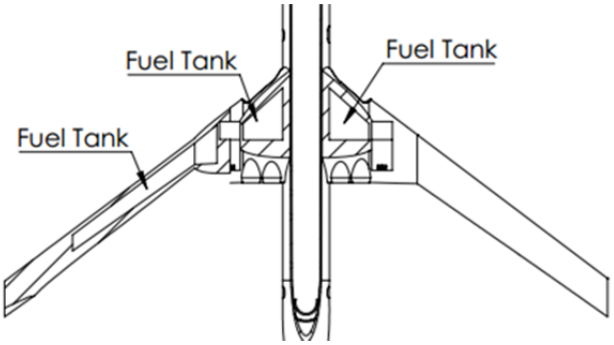

Figure 17. Wing Structure

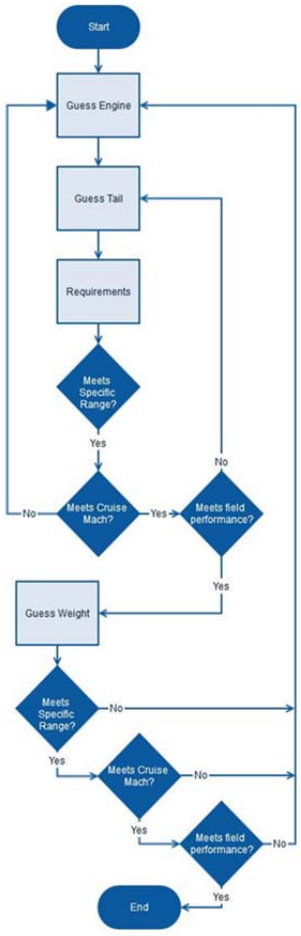

Figure 18. Weight Estimation Flowchart.

C. Weights

In order to size the aircraft properly, an accurate estimation of weight needed to be calculated. The weight of each component on the aircraft, (wing, empennage, fuselage, landing gear, etc.) was estimated using the "Torenbeek Weight Estimation Spreadsheet". An overall estimate of weight to size the aircraft was obtained by inputting the dimensions and weight of each component. An initial estimate of the aircraft was 80,000 pounds, based on averages from other regional transport competitors. Mission, takeoff, and performance studies were run to see how the aircraft performed at this weight condition. This weight estimation yielded excess cargo upon landing and therefore, weight estimate could be lowered. This weight reduction, however, resulted in changes throughout the design.

When weight was reduced, the wing area was reduced, less fuel was required for mission completion, the cruise point changed, and the thrust required from the engines was lowered. Reducing the size and weight of all these components then reduced the weight of the overall aircraft, and the size of all the components were reduced again. This cycle continued until the desired payload at landing was reached. Many times throughout the process of design, the wing sizing, extra fuel for loiter, and cruise conditions changed, which forced the cycle of weight changes to begin anew and checked against the payload needed. A visual representation of this process is shown in Figure 18.

The final weight was reached for all components and the overall aircraft after a

Downloaded by Timothy Takahashi on May 11, 2023 | http://arc.aiaa.org | DOI: 10.2514/6.2016-1029

multitude of iterations of the process described above. This weight breakdown can be found in Table 8A of Appendix A. After the weight was finalized, the detailed design of the wing and other components was able to begin. Minor adjustments, such as small changes in tail wetted area and wing thickness, could be made to the aircraft without having to restart the weight/sizing process. All weights and sizes were then detailed and finalized, while meeting the requirements for landing payload.

D. Engines

Since the main goal of the *Aeris* project was to improve upon the competition's fuel economy, the efficiency of the engines was critical. The team conducted an initial trade study evaluating the efficiency of turbojet and turbofan engines. The turbofan was determined to be a better engine choice, and a trade study was conducted evaluating the effect of increasing BPR on the specific range (Figure 19).

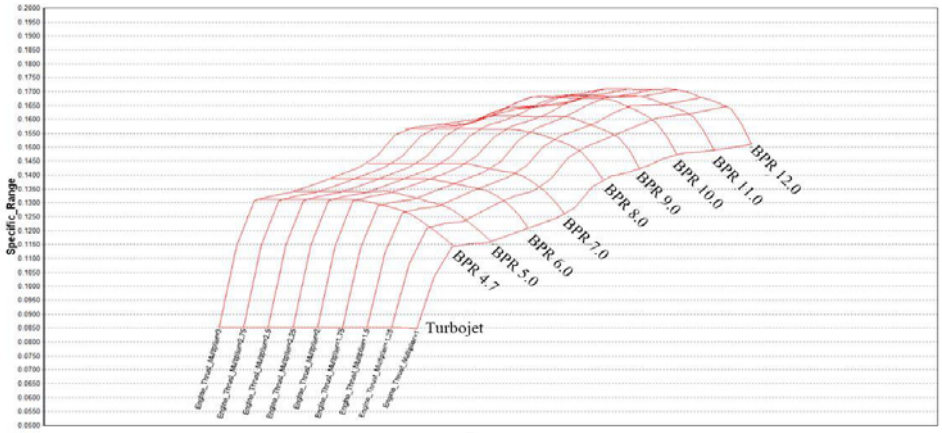

Figure 19. Specific Range vs Bypass Ratio

As demonstrated by this trade study, as the BPR increased from 4.7 to 12, the specific range increased as well. The BPR values of 10, 11, and 12 were considered because they showed the best specific range values.

Rather than the typical configuration of having two nacelle mounted engines under the wing, *Aeris* was designed to have four engines buried within the wing structure. This allowed for less wetted area due to the elimination of the nacelles, resulting in a reduction in skin friction drag. The decision to use a four engine configuration was a direct result of the wing buried engine design. To achieve the desired thrust values with two BPR 12 engines, each engine would be large in diameter and severely complicate burying the engines within the wing. In a four engine layout the resultant engine diameters made the engine integration within the wing much more practical. In order to minimize the structural impact of engine integration, the engines were placed in the wing root in close proximity to the fuselage which allowed for the engines to be integrated above the main wing spar. This resulted in large structural wing thickness, which had the effect of reducing the wing weight, and small engine offset from the fuselage centerline resulted in lower asymmetric thrust yawing moment. The yawing moment in OEI flight conditions has been addressed by an active stability system that is further discussed within the stability section of the report.

In meeting with 14 CFR 25.903, which states that one engine failure cannot cause the failure of another engine, the *Aeris*'s engines are staggered so that a rotor burst does not coincide with neighboring engines (Figure 20).

Further considerations on rotor burst also apply to 14 CFR 25.841, which states that the passengers cannot be exposed to pressure altitudes over 40,000 ft. Since *Aeris* cruises well over 40,000 ft, and the fuselage pressure

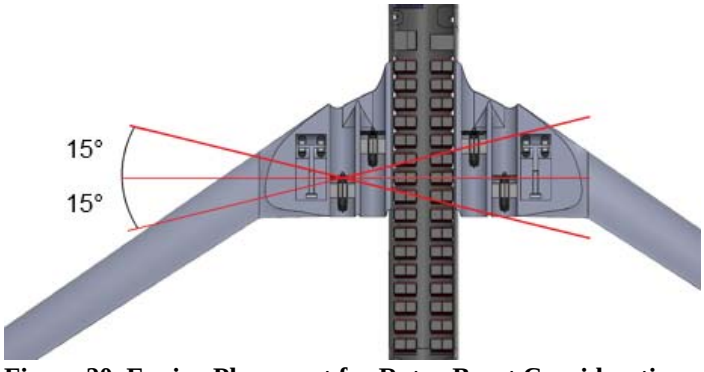

Figure 20. Engine Placement for Rotor Burst Considerations

Downloaded by Timothy Takahashi on May 11, 2023 | http://arc.aiaa.org | DOI: 10.2514/6.2016-1029

vessel lies within the rotor bust disks of all the engines, a rotor burst could potentially puncture the pressure vessel resulting in rapid decompression that exposes passengers to extreme altitudes before the plane can conduct an emergency descent. Therefore, considerations will be taken to shield the engines with ballistic armor material placed between the engines and the fuselage pressure vessel. Furthermore, because rotor burst under cruise conditions is exceedingly rare, a waiver for an exemption to this CFR will be applied for. Table 2 shows a comparison of *Aeris* engine parameters and cruise performance compared to those of regional aircraft currently in use.

Table 2. Engine Comparison.

Airplane	CRJ 700	BAE 146	E170	Q400	Aeris
MMo	.78	.73	.82	.55	**.85**
MTOW (lbs)	72,750	83,626	79,340	64,500	**65,400**
# of Engines	2	4	2	2	**4**
Thrust (lbs)	26,720	27,880	27,600	5071 SHP*	**32,000**

E. Tail

The tail and empennage played a large role in stability as well as takeoff performance. For takeoff sizing, a spreadsheet was made in order to calculate the moments about the wheels and to size the horizontal tail for rotation at stall speed (Figure 23). Weight, landing gear distance behind the center of gravity (Figure 22), and tail size were all inputs to the spreadsheet and allowed for quick calculations for tail sizing. The process is shown in Figure 21. The moments were calculated as shown in Equation 1:

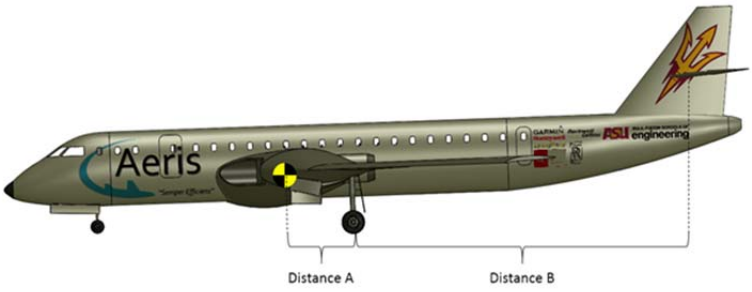

Figure 22. Distances from Center of Gravity.

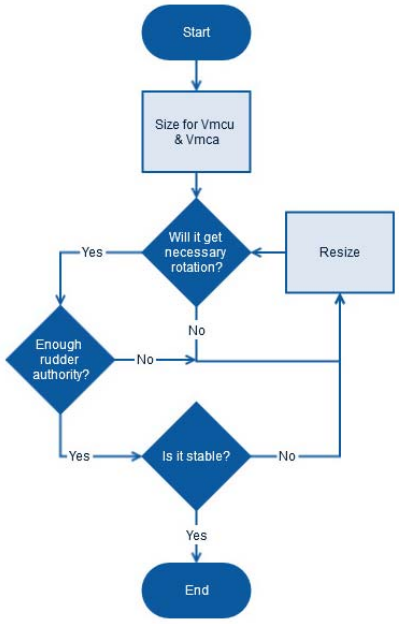

Figure 21. Tail Sizing Flowchart.

$$\sum Moments_{about\ landing\ gear} = (Aircraft\ weight * Distance_A) - (L_{tail} * Distance_B) \quad (1)$$

$$where\ L_{tail} = Cl * q * S_{ref}$$

We designed the using a symmetrical NACA 0008-34 airfoil with a maximum lift coefficient of 1. The maximum lift coefficient was assumed to occur at a maximum elevator deflection of 30 degrees. By using this C_L, the dimensional lift force could be calculated at any given airspeed. This, coupled with the moment arm of the horizontal stabilizer location on the fuselage, allowed the calculation of the moment about the main landing gear. Therefrom, the team calculated the minimum airspeed for nose wheel unstick at maximum elevator deflection.

Downloaded by Timothy Takahashi on May 11, 2023 | http://arc.aiaa.org | DOI: 10.2514/6.2016-1029

Horizontal Tail Moment		Cl_Tail	Weight	Length from wheel to CG (ft)			q_sl/M^2	V_mu/a	q=		V_mu (kts)					
		1	61400	2.25			1481.35	0.16667	41.1487		110					
Sum of moments		**Length of tail from wheel Base**														
		0	**5**	**10**	**15**	**20**	**25**	**30**	**35**	**40**	**45**	**47**	**50**	**55**	**60**	**65**
Tail S_ref -->	**50**	138150	127863	117575.64	107288	97001.3	86714.1	76426.9	66139.7	55852.5689	45565.39001	41450.51846	35278.2	24991	14703.9	4416.67
	60	138150	125805	113460.77	101116	88771.5	76426.9	64082.3	51737.7	39393.08268	27048.46802	22110.62215	14703.9	2359.24	-9985.38	-22330
	70	138150	123748	109345.9	94943.8	80541.8	66139.7	51737.7	37335.6	22933.59646	8531.546021	2770.725844	-5870.5	-20272.6	-34674.6	-49076.7
	80	138150	121691	105231.03	88771.5	72312.1	55852.6	39393.1	22933.6	6474.110243	-9985.37598	-16569.1705	-26444.9	-42904.3	-59363.8	-75823.3
	90	138150	119633	101116.16	82599.2	64082.3	45565.4	27048.5	8531.55	-9985.37598	-28502.298	-35909.0668	-47019.2	-65536.1	-84053.1	-102570
	100	138150	117576	97001.284	76426.9	55852.6	35278.2	14703.9	-5870.5	-26444.8622	-47019.22	-55248.9631	-67593.6	-88167.9	-108742	-129317
	110	138150	115518	92886.413	70254.6	47622.8	24991	2359.24	-20272.6	-42904.3484	-65536.142	-74588.8594	-88167.9	-110800	-133432	-156063
	120	138150	113461	88771.541	64082.3	39393.1	14703.9	-9985.38	-34674.6	-59363.8346	-84053.064	-93928.7557	-108742	-133432	-158121	-182810
	123	138150	112844	87537.08	62230.6	36924.2	11617.7	-13688.8	-38995.2	-64301.6805	-89608.1406	**-99730.7246**	-114915	-140221	-165528	-190834
	130	138150	111403	84656.67	57910	31163.3	4416.67	-22330	-49076.7	-75823.3209	-102569.986	-113268.652	-129317	-156063	-182810	-209557
	140	138150	109346	80541.798	51737.7	22933.6	-5870.5	-34674.6	-63478.7	-92282.8071	-121086.908	-132608.548	-149891	-178695	-207499	-236303
	150	138150	107288	76426.927	45565.4	14703.9	-16157.7	-47019.2	-77880.8	-108742.293	-139603.83	-151948.445	-170465	-201327	-232188	-263050
	160	138150	105231	72312.055	39393.1	6474.11	-26444.9	-59363.8	-92282.8	-125201.78	-158120.752	-171288.341	-191040	-223959	-256878	-289797
	170	138150	103174	68197.184	33220.8	-1755.63	-36732	-71708.4	-106685	-141661.266	-176637.674	-190628.237	-211614	-246590	-281567	-316543
	180	138150	101116	64082.312	27048.5	-9985.38	-47019.2	-84053.1	-121087	-158120.752	-195154.596	-209968.134	-232188	-269222	-306256	-343290
	190	138150	99058.7	59967.44	20876.2	-18215.1	-57306.4	-96397.7	-135489	-174580.238	-213671.518	-229308.03	-252763	-291854	-330945	-370037
	200	138150	97001.3	55852.569	14703.9	-26444.9	-67593.6	-108742	-149891	-191039.724	-232188.44	-248647.926	-273337	-314486	-355635	-396783
	210	138150	94943.8	51737.697	8531.55	-34674.6	-77880.8	-121087	-164293	-207499.211	-250705.362	-267987.822	-293912	-337118	-380324	-423530

Figure 23. Horizontal Tail Rotation Sizing

As seen in Figure 23, the horizontal stabilizer has more than enough authority for rotation at the desired unstick speed (Vmu). This effect is due to the tail needing more area for the cruise conditions. Sizing the horizontal tail and elevator area for the takeoff condition caused the trim angle of the tail to be set at 10 degrees. This high trim angle would result in the horizontal stabilizer operating at very high lift coefficients in order to generate the required downforce for trimmed flight. This would most likely result in the horizontal stabilizer operating at or near stall, if not in partial stall, resulting in high drag generation and unfavorable performance. Therefore, the team increased the tail area in order to increase the dimensional downforce for trimmed flight and reduce the necessary C_L. The horizontal tail now sits at 3.7 degrees at the cruise condition, and has more than enough control authority for takeoff. The tail surfaces were designed in a cruciform configuration in order to remove the horizontal stabilizer from the exhaust of the close coupled engines.

When sizing the vertical tail, initial design protocol would have dictated that the vertical stabilizer should have been sized in order to counter asymmetric thrust encountered in OEI flight conditions. While this is a necessary consideration on a twin engine aircraft, the *Aeris* utilizes a four engine configuration and has the advantage of being able to alter the thrust on the remaining operating engines. This thrust alteration can reduce or even null the asymmetric thrust yawing moment while maintaining climb performance. In evaluating this operating scenario, the highest asymmetric thrust condition was considered to be an engine failure on the most outboard engine station. If the aircraft remained stable and maintained the required climb gradient, scenarios of inboard engine failure were deemed to be within the aircraft's capability to counter asymmetric thrust yawing with individual engine throttling, and therefore not evaluated. This capability would have to be integrated into the FADEC and flight management system, as detection of loss of thrust on a failed engine would require immediate thrust augmentation in order to null out yawing moments before sideslip angles affected the controllability of the aircraft.

In order to evaluate the climb performance of the aircraft in OEI flight conditions with the "One Engine Inoperative Asymmetric Thrust Yawing Moment Active Thrust Augmentation Stability System" (O.E.I.A.T.Y.M.A.T.A.S.S.) active, a spreadsheet was created to evaluate the thrust values required to null asymmetric thrust yawing moments. Climb performance was then evaluated using these thrust numbers. Examining Table 3, throttle position, thrust, dead engine drag and resultant moment were all calculated and summed. This gave a nearly zero yawing moment thrust setting, which was then used to calculate climb performance. This showed a favorable climb gradient with the system active, and renders it unnecessary to size the vertical stabilizer for OEI. Further vertical stabilizer sizing was done with *VORLAX* in order to achieve appropriate directional

Table 3. OEI Performance

Second Segment Climb With Engine Thrust Adjusted to Remove Asymmetric Thrust Yawing Moment					
	Engine station 1	Engine Station 2	Engine Station3	Engine Station 4	
Span Location (ft)	10	6.25	-6.25	-10	
Throttle Setting	0.85	0.9942	1	0	
Thrust	467.5	5721.2	6377.6	-559.0	Sum of Moments
Moment	4675.2	35757.2	-39860.0	5590.0	13.4
Climb gradient	13.39%				
R.O.C. (fpm)	1935				

Downloaded by Timothy Takahashi on May 11, 2023 | http://arc.aiaa.org | DOI: 10.2514/6.2016-1029

stability characteristics. The detailed stability derivatives are presented in the Stability & Control section.

F. Landing Gear

The team ran a small trade study of the main landing gear wherein it compares 2 tire and 4 tire configurations (Table 4). The tire sizes were found using the Goodyear Tire Data Book [16], and correctly sized for the aircraft weight using the 1.07 factor of safety specified by 14 CFR 25.733 (c) (1). The team found that using 1 bogey with two tires met the requirements while weighing 170 pounds less than the 4 tire configuration.

Table 4. Landing Gear Configuration Comparison.

	2 tires x 1 bogeys	4 tires x 2 bogeys
Total Tires	4	8
Load per Tire	17494.5	8747.25
Tire	H36x12.0-18	34x10.75-16/10.50-16
Rated Load (lbs)	21,525	10,870
Weight (lbs)	82.9	62.5
Weight Total (lbs)	**331.6**	500

The landing gear had to be placed in a location that ensured the airplane would not tip backward and would remain stable while on the ground. This required the main landing gear to be placed behind the plane's center of gravity in such a manner that the angle between the main landing gear contact point and the C.G. would be greater than the required rotation angle (Figure 24). The team shortened the front landing gear strut in order to tilt the wings downward 2 degrees. This produced a zero-lift angle-of-attack while taxiing on the runway.

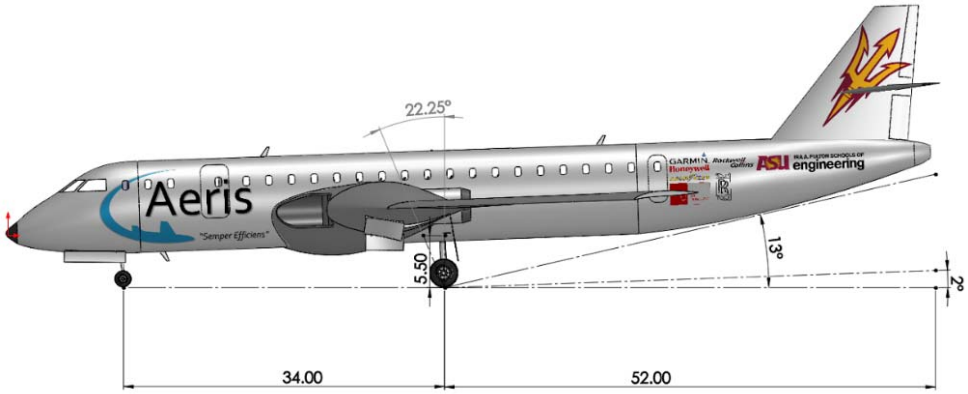

Figure 24. Landing Gear Location.

IV. Performance

A. Stability & Control

Once the final dimensions for the plane were completed, it was ran in *VORLAX* at multiple angles of attack to check the correctness of the stability derivatives. Longitudinal, directional, and lateral stability were all checked and verified to be within the required limits (Figure 25). The plots generated from these results are shown and discussed individually below.

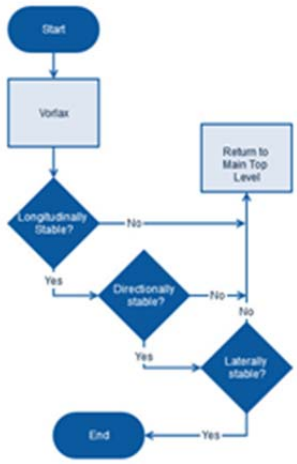

Figure 25. Stability and Control Flowchart

Downloaded by Timothy Takahashi on May 11, 2023 | http://arc.aiaa.org | DOI: 10.2514/6.2016-1029

In order to check the stability of the aircraft, a multitude of charts were used to understand the "handling qualities" of this conceptual aircraft.

The Bihrle-Weissman chart (Figure 26) is used to determine the dynamic Dutch Roll stability of the aircraft. On this chart the lateral control departure parameter (LDCP) is plotted on the y-axis with the parameter CnBdynamic plotted on the x-axis. There are seven segments on the chart, each of which correlates to a characteristic of the aircraft. The Birhle-Weissman was used as a screening tool to ensure a dynamically stable aircraft in the cruise condition.

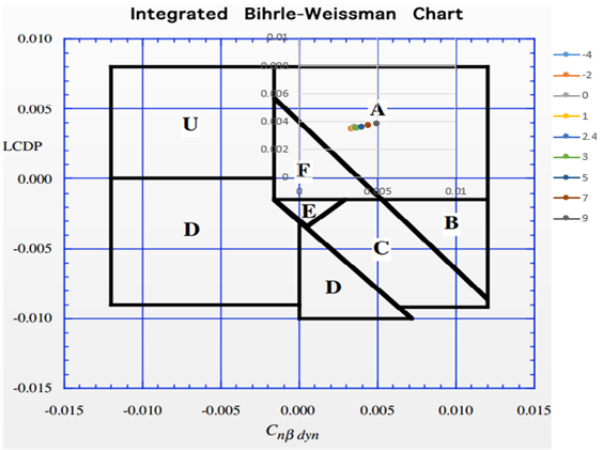

Figure 26. Bihrle-Weissman Chart.

The aircraft lands within the A range at all angles of attack, at the cruise condition, on the Weissman chart (Figure 26). The A range demonstrates the best dynamic directional stability, where the aircraft is considered highly departure and spin resistant.

In the longitudinal direction, MIL-F-8785C[17] chart (Figure 27) was used to determine the estimations of the short period frequency response of the aircraft to its pitch responsiveness. This chart provides levels which set the boundaries of these parameters to those that give a favorable flight characteristic. Therefore the aircraft is expected to fall within the given boundaries. For this aircraft, the parameters fall within the "Level 1" category which is considered the most stable category. Aircraft in this category are considered to have flying qualities adequate for the flight regime.

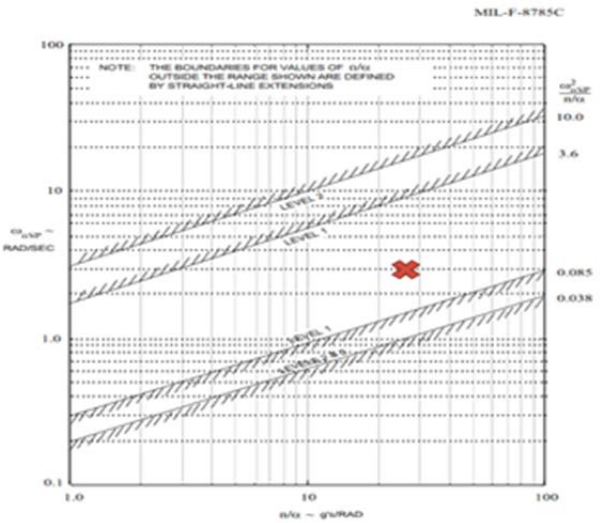

Figure 27. MIL-F-8785C Chart.

The final check for the aircraft was to determine the steady-state stability derivatives. These derivatives were determined from the pitching, rolling, and yawing moment coefficients of the aircraft at various angles of attack (therefore various lift coefficients). These coefficients were then plotted to verify that the slopes, which are the stability derivatives, to ensure the aircraft has the correct stability trends. Figure 28 (below) shows these charts for the aircraft at the cruise Mach number. These figures indicate the aircraft does indeed obtain the correct stability numbers.

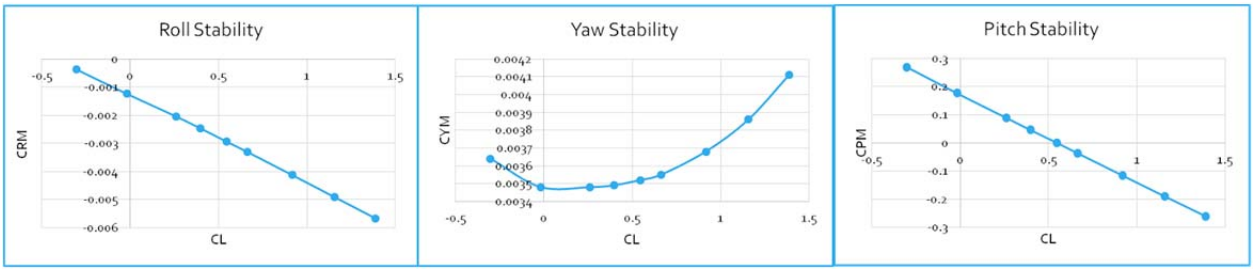

Figure 28. Roll, Yaw, and Pitch Stability.

Downloaded by Timothy Takahashi on May 11, 2023 | http://arc.aiaa.org | DOI: 10.2514/6.2016-1029

B. Point Performance - SkyMaps

SkyMaps are various plots of aircraft performance used to determine the effects of altitude and speed. These plots are developed using *EDET* and five-column thrust data, and were calibrated against the known performance of the A320. With these plots, the team could determine the efficient cruise point to fly, and even determine a starting point for the climb and decent profile of the aircraft (these were determined more in the mission profile described below). Figures 29 through 33 (below) are produced using the aircraft's maximum takeoff weight of 64,500-lbm.

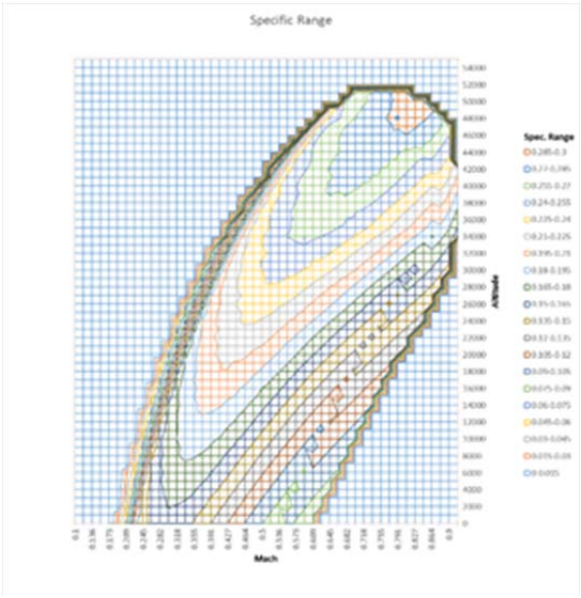

Figure 29. Skymap of Specific Range.

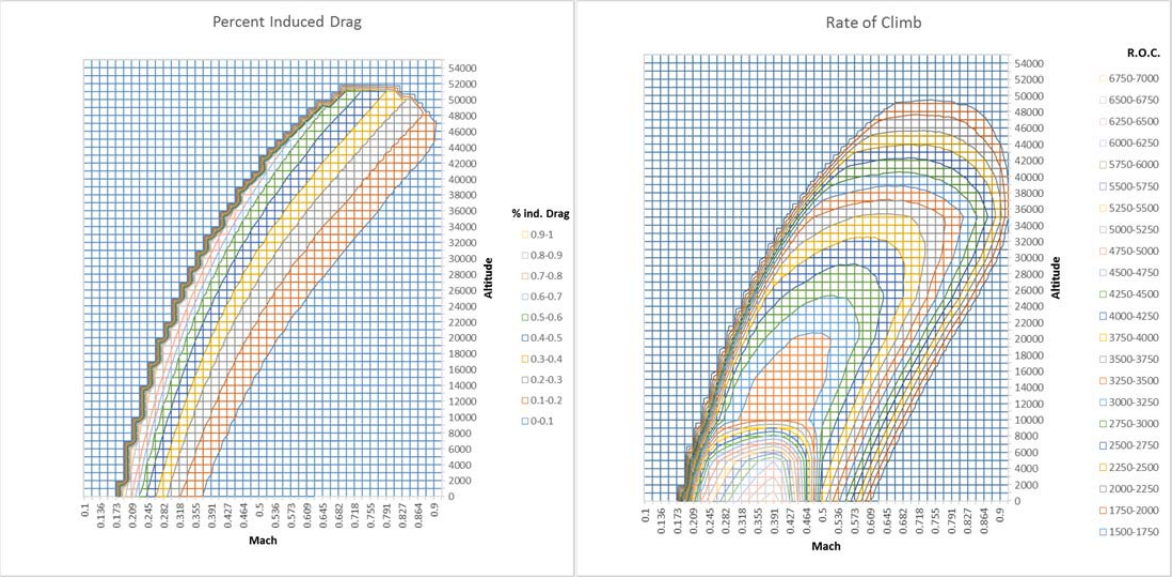

Figures 30 & 31. Skymap of Percent Induced Drag (Left) and Rate of Climb (Right).

Downloaded by Timothy Takahashi on May 11, 2023 | http://arc.aiaa.org | DOI: 10.2514/6.2016-1029

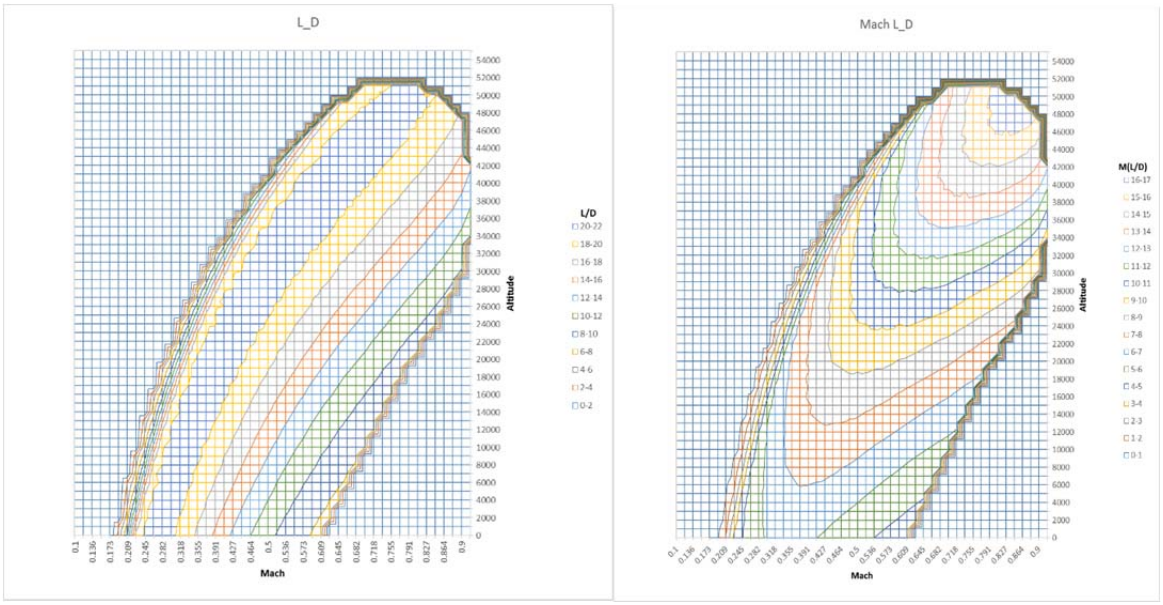

Figures 32 & 33. Skymap of L/D (Left) and M(L/D) (Right).

C. Mission

The SkyMaps above only show a screenshot of the flight performance of the aircraft. In order to determine the actual fuel burn and the performance of the aircraft in the off-design cases, a mission code was used to "fly" the airplane. The mission code used was a time step integration tool which is commanded by key words. The team built up a file of the flight patch commands to run this aircraft through the required missions. It became evident early in the process that the manner of which the aircraft flies the mission drastically altered the mission outcomes for fuel burn, time aloft, and distance traveled.

Listed below are the two main mission requirements that were set for the project.

1. "Long range mission"; 1500-nM with 15,000-lbm of payload; No fuel burn requirement.
2. "Short range mission"; 500-nM with 13,000-lbm of payload; 35-lbm of fuel burned per seat or less.

Both of the missions above include a divert, which, according to FAA regulations, is defined as a 45 minute hold at a low altitude loiter point. Before running the mission code, the amount of fuel burned during the divert and 45 minute hold needed to be calculated. The weight of this fuel would be added to the landing excess payload in order to ensure that the aircraft could complete the missions with the required fuel reserves for the divert and loiter period. It was estimated that in a 45 minutes hold, approximately 250-nM would be covered, which was substantially more than a 100-nM alternate. The maximum fuel burn for the aircraft was during the long range mission and 45 minute hold condition. The team used this condition as the baseline for the minimum amount of fuel the aircraft could carry in the fuel tanks.

The fuel burn for the loiter was calculated using the SkyMaps code. The team adjusted the code to represent the aircraft near landing weight. It was found that at 5000-ft., and 0.3 Mach, the fuel burn was 1024-lbm/hr. Equation 2 shows this solved the fuel burn over 45 minutes.

$$\frac{1024lb}{hr} * \frac{1\,hr}{60min} * \frac{45min}{1hr} = 768lbs\ burned\ in\ 45\ min \quad (2)$$

Following these calculations, the team designated 1,000-lbm as the necessary fuel for the divert and hold conditions. Adding this 1000-lbm to the payload needed for the shorter and longer range mission yields a payload weight at landing of 14,000-lbm and 16,000-lbm, respectively. Upon landing, this payload needed to be accounted for in the aircraft, since it accounts for all of the cargo, passengers and extra fuel. This extra payload would size the landing weight as well as the takeoff weight. The process carried on through many iterations to pinpoint the exact weight as

Downloaded by Timothy Takahashi on May 11, 2023 | http://arc.aiaa.org | DOI: 10.2514/6.2016-1029

the missions were changed.

The first optimized parameter of the mission code was the takeoff and climb. Based off of the SkyMaps code, the team found that a 210 KIAS climb out was optimal for minimum fuel burn. The 210 KIAS climb was held at full throttle until 42,000-ft. This was followed by constant Mach climb at 0.83 Mach to the cruise altitude of 50,000-ft. This climb out procedure was used for the long range mission where there was time and distance for the aircraft to climb to an optimal altitude. The shorter mission held the same climb out procedure but only ascended to 37,000-ft. Due to the amount of fuel used to climb, it was discovered to be inefficient to climb 50,000-ft (the optimal cruise altitude of the aircraft). Therefore the aircraft would be less efficient at its lower altitude cruise point, but this slight inefficiency is offset by the lower fuel burn during the climb out. Many takeoff and climb profiles were built around the procedure described above, however each alterative climb profile resulted in a higher fuel burn.

The team found the minimum fuel burn for cruise was found to be at 0.83 Mach throughout the long range mission. For the short range mission, 210 KIAS, or 0.68 Mach, was maintained at 37,000-ft for minimum fuel burn. This cruise altitude was found using an iterative method for minimum fuel burn. The final optimization of this mission profile was done by hand due to the distance of the mission changing slightly depending on the cruise altitude, distance, and speed.

The descent profile was the largest source of variation in calculating and optimizing fuel burn. Through the use of iterative optimization methods, the team found that it was most efficient to make decent as quick as possible in order to remain at the efficient high altitude cruise. This driving concern was due to the fact that the engines burned more fuel at idle at lower altitudes than at cruise power and cruise altitude. In order to simulate increased drag from airbrake/spoiler deployment, 200 counts of drag was added at the beginning of descent. This provides the aircraft with the ability to descend quickly without over-speeding. For the short range mission, only 26 counts of drag were added, due to the use of a more shallow descent. Both missions modeled the aircraft descended at 220 KIAS. During the optimization of the decent profile, the variations in drag (therefore speed brake/spoilers deployment), caused vast variations in the total mission performance. The required finesse in determining the proper flight profile became simpler to complete through trial and error over an automated process. Visual representations of the missions are shown below:

Weight Initial	65400 lbm
Weight Final	59586.75 lbm
MLW	60000 lbm
Total Mission Time	3hr 25min
Total Dist Flown	**1509.36 nm**
Excess Payload	**16019.75 lbm**
Fuel Burned	5813.52 lbm

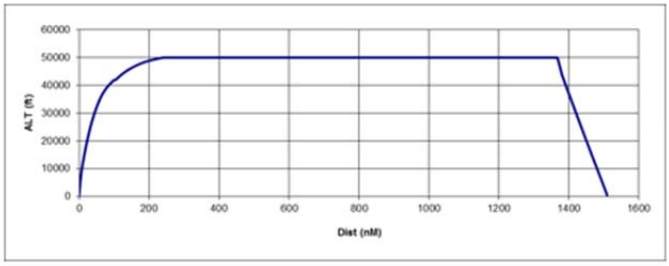

Figure 34. Mission 1: Long Range with Loiter.

Weight Initial	65400 lbm
Weight Final	58987.87 lbm
MLW	60000 lbm
Total Mission Time	3hr 51min
Total Dist Flown	**1606.51 nm**
Excess Payload	**15420.87 lbm**
Fuel Burned	6412.30 lbm

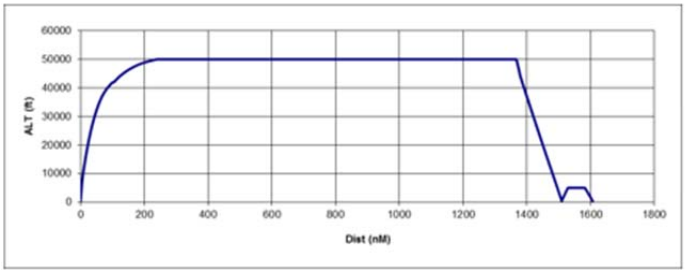

Figure 35. Mission 2: Long Range with Divert.

Downloaded by Timothy Takahashi on May 11, 2023 | http://arc.aiaa.org | DOI: 10.2514/6.2016-1029

Weight Initial	59950 lbm
Weight Final	57534.28 lbm
MLW	60000 lbm
Total Mission Time	1hr 33min
Total Dist Flown	**505.95 nm**
Excess Payload	**14016.94 lbm**
Fuel Burned	2365.50 lbm

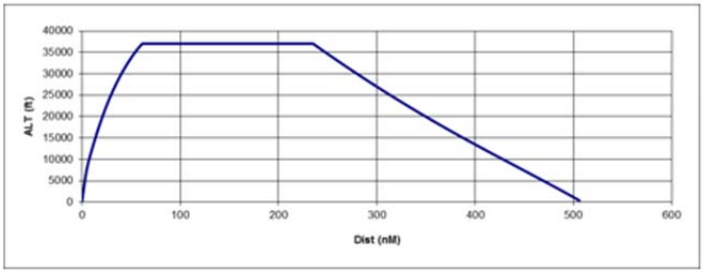

Figure 36. Mission 3: Short Range with Loiter.

Weight Initial	59900 lbm
Weight Final	56952.11 lbm
MLW	60000 lbm
Total Mission Time	1hr 57 min
Total Dist Flown	**600.28 nm**
Excess Payload	**13385.11 lbm**
Fuel Burned	2947.69 lbm

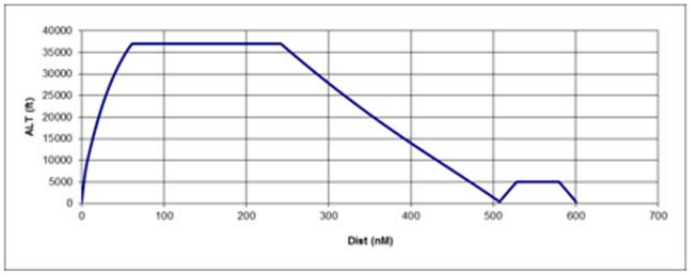

Figure 37. Mission 4: Short Range with Divert.

In order to meet the 35-lbm of fuel burn per seat, the short range mission was run with the included loiter. The team found the total fuel burned in this mission to be 2365.5-lbm. Calculating the fuel burn per passenger (Equation 3) results in 33.79-lbm per seat, exceeding the requirement.

$$\frac{2365.5\ lbm}{70\ passengers} = \frac{\mathbf{33.792}lbm}{passenger} \quad (3)$$

For additional comparison to competitive aircraft, the team calculated a maximum range mission and a payload range chart (Figures 38 & 39, respectively). The aircraft, was found to have a ferry range of 4,200-nM with a specific range of .324. This aircraft not only meets the requirement for a short range mission, but improves as the missions become longer due to the ability to remain at the efficient high altitude cruise condition. With the capabilities shown as a regional jet, variant of this aircraft could also be considered for other uses i.e. military, search and rescue, or long range private jet. Such variants would have larger fuel tanks, and a restricted maximum payload to accommodate longer missions and loiter times. The maximum mission profile is shown below in Figure 39.

Weight Initial	56481lbm
Weight Final	43536.7 lbm
MLW	60000 lbm
Total Mission Time	9hr 3min
Total Dist Flown	4214 nm
Excess Payload	33.16 lbm
Fuel Burned	12967 lbm

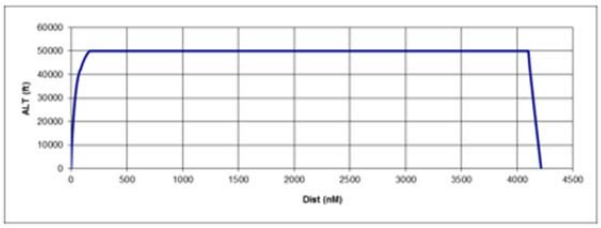

Figure 38. Mission 5: Ferry Range.

Downloaded by Timothy Takahashi on May 11, 2023 | http://arc.aiaa.org | DOI: 10.2514/6.2016-1029

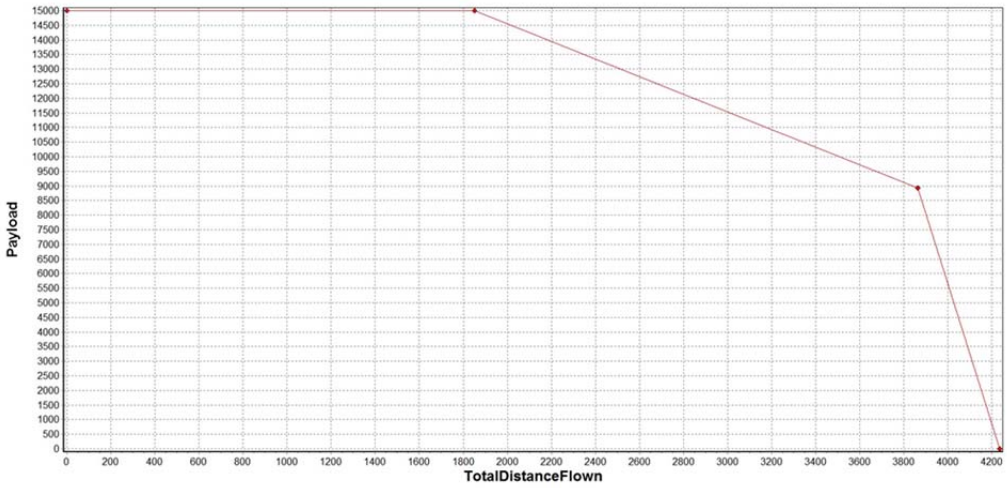

Figure 39. Payload - Range Chart.

D. V-N Diagram

The team created a V-N Diagram (Figure 40) to show the flight envelope of the aircraft. This diagram also demonstrates the change in performance when the flaps are extended.

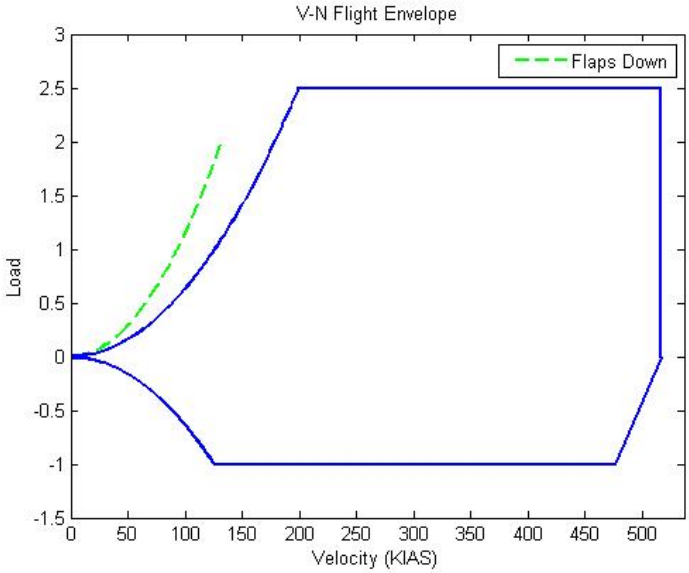

Figure 40. V-N Diagram.

E. Final Aircraft Configuration

The 3-View drawing of the final configuration is shown below in Figure 41. The full geometric measurements of the aircraft can be found in Appendix A. All dimensions in the drawing below are in feet unless otherwise specified.

Downloaded by Timothy Takahashi on May 11, 2023 | http://arc.aiaa.org | DOI: 10.2514/6.2016-1029

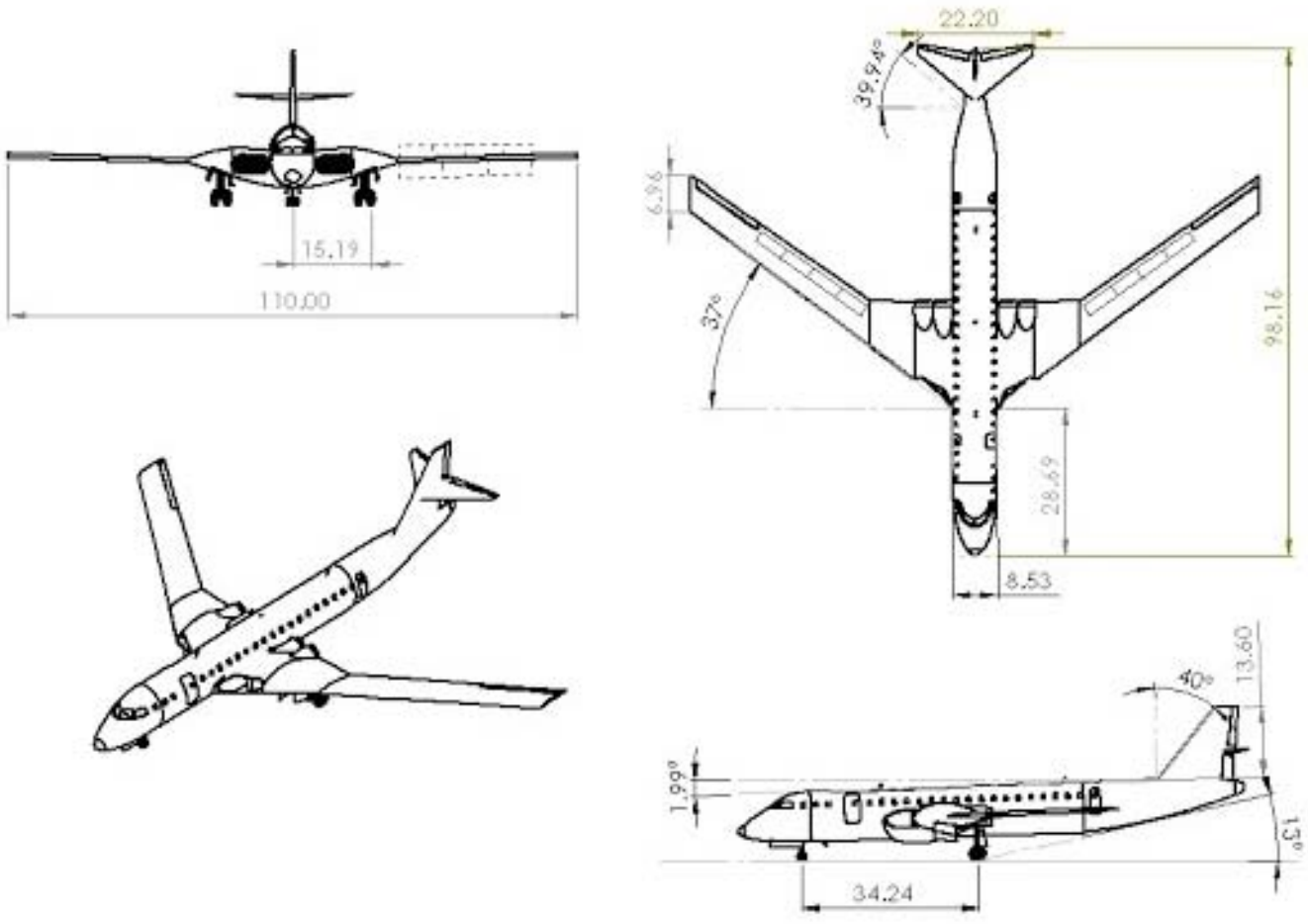

Figure 41. 3-View Drawing.

This aircraft was designed to compete with regional jets currently on the market. A side by side comparison of the *Aeris* aircraft and its competition is shown below in Table 5. The current market aircraft being compared are the Embraer E-170[18], Bombardier CRJ-700[19], Bombardier Q400[20], and the British Aerospace 146 [21].

Table 5. Comparison to Competitors.

	E-170	CRJ-700	Q400	BAe146	*Aeris*
Seating Capacity	70	66	68	68	70
Range (-nM)	1,800	1,218	1,567	1,570	1,850
Service Ceiling (ft)	41,000	41,000	27,000	35,000	51,000
Cruise Mach	0.82	0.78	0.55	0.73	0.83
Payload Capacity (lbm)	20,000	18,800	19,114	20,943	16,000
Fuel Capacity (lbm)	20,580	19,592	11,729	20,787	13,000
OEW (lbm)	46,610	43,449	37,886	52,580	43,567
MTOW (lbm)	79,340	72,750	64,500	83,626	65,400
Specific Range	0.14	0.12	0.21	0.16	0.29

Downloaded by Timothy Takahashi on May 11, 2023 | http://arc.aiaa.org | DOI: 10.2514/6.2016-1029

V. Conclusion

After exploring the merits of speed against efficiency, it is shown that an aircraft can achieve both. Overall, the team designed the aircraft toward efficiency, but in the process created an airplane that attains high cruise speeds as well. When compared against the current market competitors (Table 5 above), the *Aeris* achieves both the highest speed as well as the best specific range. It maintains a cruise Mach of 0.83, when the next fastest competitor, the Embraer E-170, flies at 0.82. The overall difference in Mach number may not be large, but this is also coupled with more than double the specific range. The E-170 has a specific range of 0.14, as compared to the 0.29 of the *Aeris*. If looking purely at efficiency through specific range, the best current market competitor is the Bombardier Q400, with a specific range of 0.21. The specific range of the *Aeris* is .29, while cruising at a Mach of 0.83 to .55 for the Q400.

The reason for this significant performance improvement comes down to two main factors. The first factor is the low drag design. The fuselage is sized to minimize the total drag while still being practical. The shape and twist of the wing to a near elliptical lift distribution minimizes the induced drag during cruise. The burying of the engines within the wing eliminated the drag from additional wetted area and unfavorable airflow effects over the wing brought upon by nacelles.

The second main factor in improved performance is the way the aircraft is flown. As previously shown, the aircraft cruises at a much higher altitude than the other competitors. The operational ceiling of the *Aeris* is 10,000 ft higher than the next best competitor. The aircraft is optimized to this altitude, and from this sees great performance improvements. Due to the thin atmosphere at this altitude, the engines operate at high efficiencies and the airframe experiences less drag. The *Aeris* burns more fuel at low altitude with the engines at idle than it does at full throttle when at cruise altitude. This increase in altitude is not without its drawbacks, however, this altitude may require special exemptions from the FAA. CFR requirements state that passengers may not be exposed to altitudes of over 40,000 ft for any length of time. Due to the engine configuration on the *Aeris,* a rotor burst poses a real threat to puncturing the passenger compartment pressure vessel. In the past, however, the FAA has granted exemptions to this rule due to the extreme rarity of rotor burst. Even if the aircraft is proven safe, the authorities are not required to grant the exemption. In this project the team worked under the assumption that this waiver would be granted, but ultimately that decision would rest in the hands of the FAA.

Overall, this aircraft met or exceeded every requirement set forth for it. It outperforms market competitors and while meeting federal regulations. All aspects of an aircraft design are intertwined and a change in one area can cause changes in all others. Speed and efficiency are not on opposite ends of a teeter totter, they are peddlers on a tandem bicycle.

Downloaded by Timothy Takahashi on May 11, 2023 | http://arc.aiaa.org | DOI: 10.2514/6.2016-1029

Appendix A

Table 1A. Fuselage

Length	98 ft
Width	8.5 ft
Height	9.7 ft
Fineness Ratio	10.8

Table 2A. Cabin

	First Class	Coach Class
Seating Layout	2+1	2+2
Seat Width	21 in	17.4 in
Seat Pitch	31 in	30 in
Aisle Width	21.4 in	20 in
Number of Passenger Seats	6	64

Table 3A. Wing

Span	110 ft
Reference Area	930 ft^2
Wetted Area	1977 ft^2
Aspect Ratio	13
Root Chord	20.75 ft
Tip Chord	7 ft
Average Wing Thickness	11.8%
Cl max (clean)	1.31
Cl max (landing)	2.41
Taper Ratio	0.7
Sweep	37 degrees
Airfoil	NACA 6 Series

Table 4A. Vertical tail

Span	14 ft
Reference Area	151 ft^2
Thickness	8%
Root chord	15.5 ft
Taper Ratio	0.3
Sweep	40 degrees
Airfoil	NACA 0008-34

Table 5A. Horizontal tail

Span	22.3 ft
Reference Area	124 ft^2
Thickness	8%
Root chord	9.25 ft
Taper Ratio	0.2
Sweep	40 degrees
Airfoil	NACA 0008-34

Table 6A. Propulsion

Number of Engines	4
Thrust per Engine (Static Sea-Level)	8,000 lbs
Bypass Ratio	12
Fan Diameter	38.46 in

Table 7A. Landing gear

	Nose	Main
Number of struts	1	2
Number of tires	2	4
Position (aft of nose)	12 ft	47 ft
Length of Struts	5.8 ft	7 ft
Wheel base	34 ft	

Downloaded by Timothy Takahashi on May 11, 2023 | http://arc.aiaa.org | DOI: 10.2514/6.2016-1029

Table 8A. Weights and performance

MTOW	65,400 lbs
MLW	60,000 lbs
MZFW	58,567 lbs
OEW	43,567 lbs
BEW	42,789 lbs
MEW	39,903 lbs
Cruise Mach	0.83
Cruise Altitude	50,000 ft
T/W	0.49

References

[1]Jet Transport Performance Methods, Boeing Flight Operations Engineering, D6-1420, 7th Ed., May 1989

[2]Southwest Airlines FAA Approved Flight Manual – Boeing 737 Family Airliners, Southwest Airlines, 1995 edition.

[3]Capone, F.J., "Wind Tunnel/Flight Data Correlation for the Boeing 737-100 Transport Airplane", NASA TM X-72715, August 1975.

[4]737 Airplane Characteristics for Airport Planning, Boeing Commercial Airplanes, D6-58325-6, Sep. 2013.

[5]747 Airplane Characteristics for Airport Planning, Boeing Commercial Airplanes, D6-58326, May 1984.

[6]Hanke, C.R. and Nordwall, D.R., "The Simulation of a Jumbo Jet Transport Aircraft. Volume II: Modeling Data", D6-30643, Sep. 1970.

[7]Public Laws of the United States of America Passed at the Sixty-Ninth Congress 1925-1927, § 344 (1926). Print.

[8]Torenbeek, E., Synthesis of Subsonic Airplane Design, Delft University Press, Delft, Holland, 1982

[9]Miranda, L. R., Baker, R. D., and Elliott, W. M., "A Generalized Vortex Lattice Method for Subsonic and Supersonic Flow", NASA CR 2875, 1977.

[10]14 C.F.R. § 25 et seq. 2014.

[11]Donovan, Shane M., and Timothy T. Takahashi. *A Rapid Synthesis to Develop Conceptual Design Transonic Wing Lofts*. Tech. El Segundo: Northrop Grumman Corporation, n.d. Print.

[12]Takahashi, Timothy T., Derek J. Dulin, and Christopher T. Kady. *A Method to Allocate Camber, Thickness and Incidence on a Swept Wing*. Tech. N.p.: n.p., 2014. Print.

[13]Pearcey, H. H. *The Aerodynamic Design of Section Shapes for Swept Wings*. Tech. Teddington: Aerodynamics Division, National Physical Labaratory, n.d. Print.

[14]Numbers, Kieth. *Hypersonic Propulsion System Force Accounting*. Tech. Wright Airforce Base: Wright Laboratory, n.d. Print.

[15]Wenzinger, Carl J. *Wind-Tunnel Investigation of Ordinary and Split Flaps on Airfoils of Different Profile*. Tech. no. 554. Langley Field: National Advisory Committee for Aeronautics, 1935. Print.

[16]Goodyear Tire and Rubber Co. *Aircraft Tire Data Book*. 2002. Raw data. 1144 E Market St, Akron, Ohio.

[17]MIL-STD 8785-C, (1980), ("Flying Qualities of Piloted Airplanes")

[18]"Embraer 170." *Embraer - Commercial Aviation*. Embraer S.A., n.d. Web. 2014.

[19]Bombardier Commercial Aircraft. *Fact Sheet CRJ700 NextGen*. Canada: Bombardier, 2014.

[20]Bombardier Commercial Aircraft. *Fact Sheet Q400 NextGen*. Canada: Bombardier, 2014.

[21]Jane's Information Group. *Jane's All the Worlds Aircraft*. 1993-1994 ed. London: Sampson Low, Marston, n.d.

[22]Takahashi, T.T., *Aircraft Peformance & Sizing Vol I & II*, Momentum Press, (in press), 2015.

[23]NPSS, Numerical Propulsion System Simulation, Software Package, Ver. 2.3.0.1, Ohio Aerospace Institute, Cleveland, OH, 2010.

Downloaded by Timothy Takahashi on May 11, 2023 | http://arc.aiaa.org | DOI: 10.2514/6.2016-1029